THE EFFECT OF REFLECTIVE BAFFLES ON THE THERMAL GRADIENT IN DIRECTIONAL SOLIDIFICATION

By

James Edward MacDonald

A thesis submitted to the University of Birmingham for the degree of

MRes in THE SCIENCE AND ENGINEERING OF MATERIALS

UNIVERSITY OF BIRMINGHAM

Department of Metallurgy and Materials

University of Birmingham

September 2011

Abstract

Analysis of the heat transfer in the DS furnace allowed the development of a numerical model to calculate radiation and conduction in the furnace for the purpose of investigating the use of low emissivity, reflective baffles in place of traditional graphite foil material to provide a more effective radiation barrier. The potential improvements on thermal gradient that can be achieved have been calculated and experimental data has been obtained, with reflective copper baffles exhibiting improved thermal gradients in the furnace at 1000^{o}C. The potential effect on the microstructure of a turbine blade if this theory were to be applied to the casting process has been predicted. A copper baffle with water cooling has been tested beyond its melting point at 1300^{o}C and a design was proposed for a copper baffle with improved water cooling that should allow operation at temperatures used in turbine blade casting of around 1600^{o}C.

Dedication

I could not have completed this work without my parents who have always shown me incredible support across all aspects of my life, allowing me to be where I am now. My father passed away when I was age 15 and it fills me with great sadness he is not here to see the completion of my MRes. I dedicate this work to his memory and to my mother, who has always put up with me, been there for me and guided me in the tough years that followed. I am eternally grateful for their love and support.

Attending Birmingham University really helped me to find my direction and get my life on track. I am honoured to have spent 5 years there developing as a person and a professional and meeting many amazing friends along the way. Along with the rest of my friends and family this has all made me the person I am today. If you love me then I love you and this is for you.

Acknowledgements

I am wholeheartedly grateful to Dr. Mark Ward who provided me with the opportunity to conduct my research. Further thanks to Dr. Ward for encouraging me, guiding me and offering constant support throughout my time at Birmingham. His continued dedication and enthusiasm has been amazing to work around and has helped immensely in the completion of my MRes.

I would also like to mention Professor Nick Green for offering backing and guidance to my project, Pete Cranmer whose knowledge and help in the foundry was vital and another student Abhay Soorya who worked on the part of the modelling code used in this project.

Contents:

List of figures:

List of tables:

1.0 – LITERATURE REVIEW

1.1 - Introduction:

Components for high temperature gas turbine applications utilise nickel-based superalloys as they exhibit very good mechanical properties and oxidation resistance at temperatures close to their melting point. Some turbine engine components must withstand gas temperatures exceeding the melting point of the alloys. The strength and durability of these is limited by the operating temperatures so producing components with better properties is desired for improved performance and service life.

The introduction of the Bridgman technique in the 1920s revolutionised the production process as it led to the development of directional solidification (DS), forming the basis for all modern DS growth techniques. This led to a number of variations on the DS process, notably the high rate solidification (HRS) process pioneered by Versnyder and Shank in 1970 and the liquid metal cooling (LMC) process developed by Giamei and Tschinkel, 1976 (Reed, 2006, p.123; Toloraiya et al., 2002).

Single crystal (SX) casting is used for blades with the highest property requirements (Gell et al., 1980), achieved typically with a pig-tail shaped spiral grain selector at the base of a mould used in a DS casting process, (Esaka et al., 2005; Dong, 2007; Dai et al., 2011) though seed crystals can also be used (Toloraiya et al, 2002; D'souza et al, 2005). To grow the structure in the <001> direction (preferential for all FCC alloys) and align this with the maximum load direction in operation minimises the strain on it during thermal cycling and allows the best creep and thermal shock properties to be

obtained. Figure 1.1 illustrates the single crystal structure compared to the grain boundaries found in equiaxed and directionally solidified components. Further information on the grain structures and orientation of different types of casting can be found across much of the literature, notably by Esaka et al. (2005), Dong (2007), Kermanpur et al. (2008) and Seo et al. (2009).

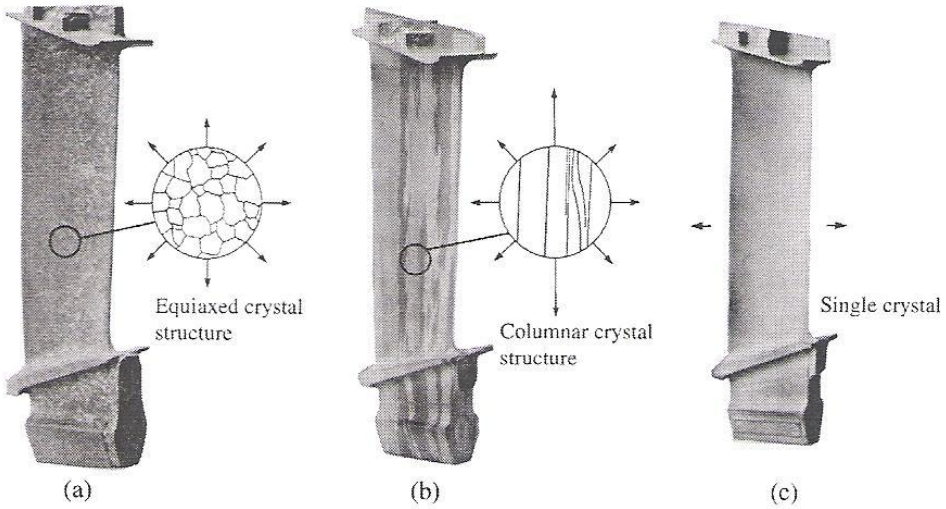

Fig. 1.1. The microstructure of turbine blades with:
a) Equiaxed, b) Directionally solidified, c) SX structures
(Reed, 2006, p.20)

1.2 – The DS casting process:

DS/SX furnaces can vary, but in principle they all work the same way. Commercially, an investment casting process is used to produce multiple components simultaneously. The furnace at Birmingham University, which can be seen in figures 1.2 and 1.3, is a Retech single shot DS furnace that uses a HRS cooling system.

Fig. 1.2. The Retech single shot DS furnace at Birmingham University, donated by Rolls Royce plc.

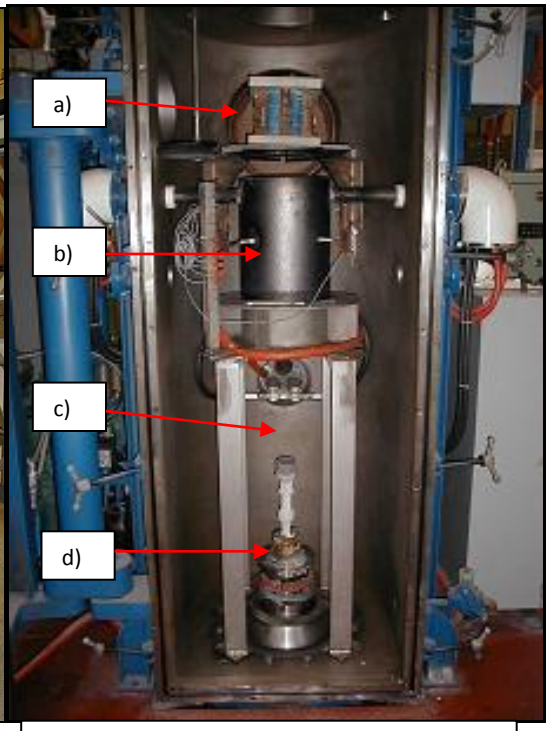

Fig. 1.3. Inside the furnace: **a)** melting coil; **b)** hot zone; **c)** cold zone; **d)** mould and chill plate.

A wax model is created exactly replicating the blade to be cast, incorporating any internal cooling passages in the design. A mould shell is then produced by dipping the models into ceramic slurries of zircon ($ZrSiO_4$), alumina (Al_2O_3) and silica (SiO_2) and firing them. The mould is preheated and degassed then molten superalloy is poured under vacuum at roughly 1550^{o}C. The component solidifies and the mould and internal ceramic core are removed by chemical processing leaving a hollow aerofoil. This alone yields superior quality blades to any wrought process as it allows components with complex internal cooling passages to be produced consistently (Reed, 2006, p.127; Liu et al., 2010). Examples of such cooling passages are shown in figure 1.4, illustrating the complex nature of the designs. The image shows single pass cooling on the left and multiple pass 'serpentine' cooling on the right.

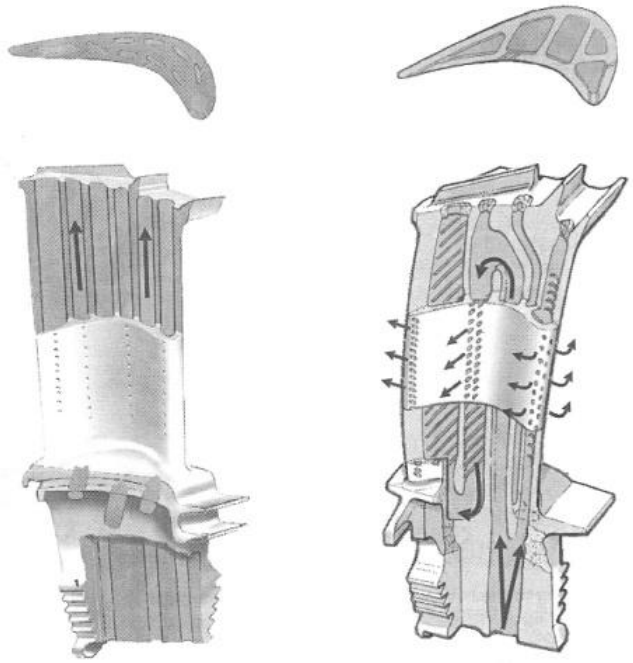

Fig. 1.4. Cross section of a turbine blade showing an example of the complex cooling channels that can be produced (Reed, 2006,

The DS process incorporates an upper melting chamber, a heating zone and cooling zone in the furnace (see labels in figure 1.3) which are pumped to cast the blade under a vacuum. The superalloy charge is loaded into a disposable crucible at the top where it is melted (relatively quickly) by a high frequency induction melting coil. Below the melting chamber is a central mould chamber surrounded by insulation (hot zone) where graphite resistance heating elements preheat the ceramic mould and heat the molten charge when it is poured in from the top crucible, to maintain it above its liquidus temperature. The hot and cold zones are separated by a radiation barrier (thermal baffle). A schematic of a DS furnace using high rate solidification, similar to that at Birmingham is shown in figure 1.5.

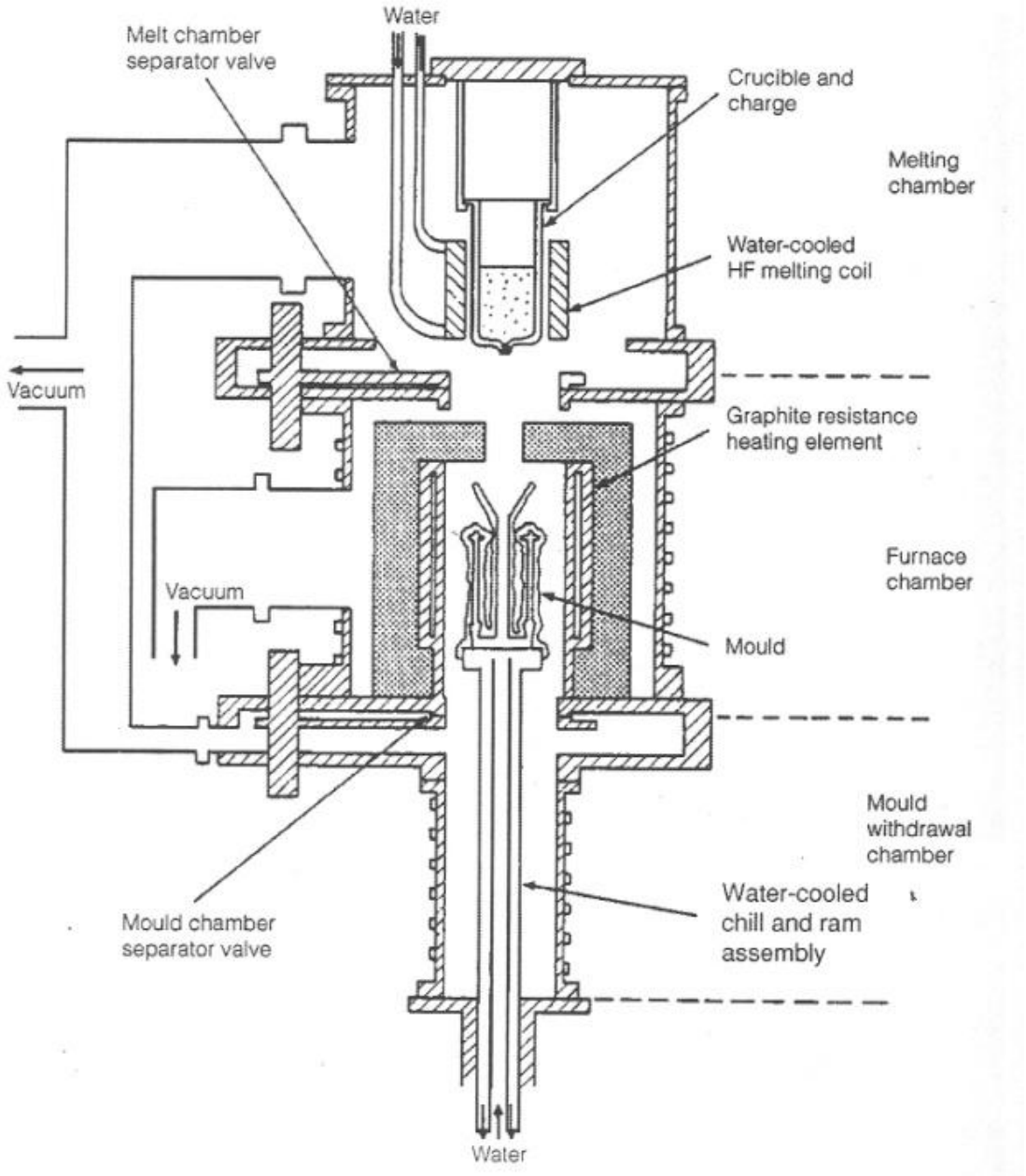

Fig. 1.5. Schematic diagram of the Bridgman DS casting technique with a high rate solidification cooling system (Reed, 2006, p.126).

After pouring the ram lowers to withdraw the mould from the heating zone at a controlled rate (as in the conventional Bridgman crystal growing method) through a gap in the baffle to a lower withdrawal chamber (cold zone), inducing directional solidification as the temperature drops below the liquidus. The withdrawal produces a thermal

gradient along the vertical axis of the casting causing solidification to occur in the direction of withdrawal, consequently making the blade stronger in the direction of the centrifugal forces developed in the gas turbine engine (Reed, 2006, p.122-123; Liu et al., 2010; Dong, 2007). Figure 1.6 shows a simplified version of DS and how the temperature field changes as the component passes into the cold zone and drops below its liquidus temperature.

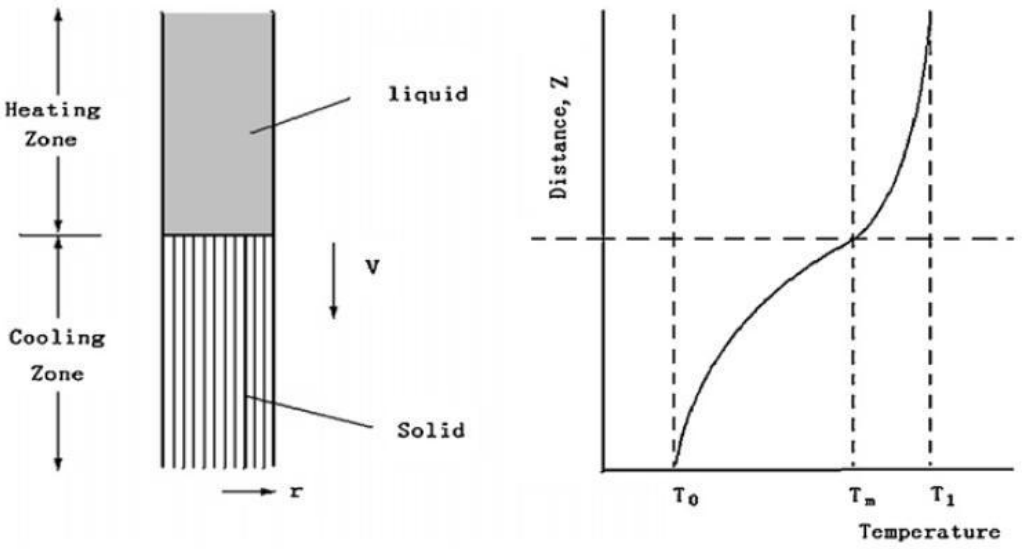

Fig. 1.6. Simplified version of DS process (left), with the temperature field (right) (Liu et al., 2010).

1.2.1 - Temperature gradient vs withdrawal velocity:

In general the DS/SX process has two major parameters controlling it - the thermal gradient G_L (K/m) and the withdrawal velocity v (m/s). Typically a high thermal gradient and low withdrawal rate are beneficial for DS structures, although it is necessary to achieve matched states between the two parameters (Reed, 2006, p.134; Liu et al., 2010), in particular to ensure the solid/liquid (s/l) interface progresses gradually along the casting, from the base upwards. A typical range of speeds used in HRS is $1x10^{-5}$-$15x10^{-5}$

ms^{-1} (Wang et al., 2003; Elliot et al., 2004) although the speed that can be achieved is dependent on the thermal gradient present. Higher thermal gradients can afford faster withdrawal velocities (hence faster solidification rates), which are beneficial for productivity, reducing chemical reaction between the mould and superalloy and reducing mould creep and cracking problems (Elliot et al., 2004). The current work has focused on a withdrawal velocity of $6.5x10^{-5}$ ms^{-1}.

1.2.2 - Role of the thermal baffle

The thermal baffle controls the thermal gradient in DS as it is the barrier that separates the hot and cold zones of the furnace, minimising radiation entering the cold zone and hindering cooling. Typically a baffle is made from graphite foil which has very low heat conduction properties (at least perpendicular to the heat flow in DS – lateral conduction through the baffle is higher) (Elsden, 2010). It is normally located on top of an insulation baffle (both of which rest on an insulation ring that forms the base of the hot zone) although this depends on the setup of the specific process e.g. some LMC variations use floating baffles (Elliot and Pollock, 2007).

1.3 - Casting size & cooling medium:

There has been extensive investigation into various cooling methods to improve the G_L. Versnyder's addition of HRS to the Bridgman technique gives improved cooling via a water cooled chill plate at the base of the mould, allowing conductive and radiative cooling to occur promoting an elevated thermal gradient. Similarly other cooling medium

have been investigated e.g. liquid metal cooling (LMC) where a liquid metal bath in the cold zone replaces some if not all radiative cooling (Kermanpur et al., 2000; Elliot et al., 2004; Elliot and Pollock, 2007; Zhang and Lou, 2007). Other methods such as water sprays, gas cooling (GCC) (Konter et al., 2000) and fluidised bed quenching (FBQ) methods (Liu et al., 2010) have been investigated as well. These all utilise conductive and convective cooling instead of/in combination with radiative cooling and depend upon close contact of the mould with the cooling medium. Of all of these, the LMC technique using molten tin is most likely to replace HRS in commercial furnaces and has already been used in Russia with improved thermal gradients achieved (Bondarenko and Kablov, 2002; Zhang and Lou, 2007). The HRS and LMC processes are shown in figure 1.7, illustrating how conduction and convection cooling in the liquid metal bath take over from radiation heat transfer in the HRS cooling zone.

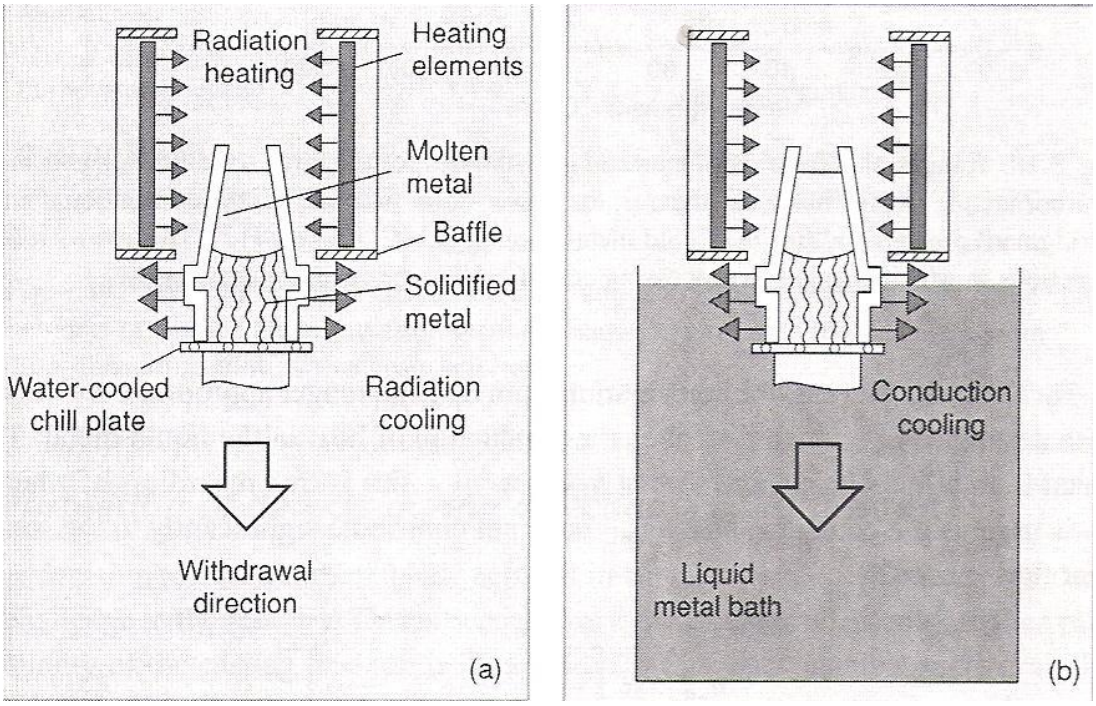

Fig. 1.7. (a) HRS with radiative cooling; (b) LMC with conductive and convective cooling (Reed, 2006, p.137).

1.4 - The importance of thermal gradient in DS:

Control of the thermal gradient is crucial in DS as the quality of turbine components is imperative and any defects are unacceptable, with higher G_L improving the quality of the structure and allowing reduced solidification time. The typical gradients (K/s) achieved with the Bridgman process give low solidification rates (m/s) and cooling rates (K/s) (where the cooling rate is defined as the product of thermal gradient and solidification rate), resulting in a coarse dendritic structure with considerable segregation and porosity (Bondarenko and Kablov, 2002; Reed, 2006, p146-147; Liu et al., 2010; Duan et al., 2010). G_L control is especially vital in the casting of larger components as it is known to decrease with increasing casting radius (r). Also with larger castings it is increasingly difficult to keep the s/l interface flat and they are more prone to defect formation (Elliot et al., 2004).

The specific reasons for increasing G_L include control of: dendrite arm spacing (Bondarenko and Kablov, 2002), the solidification front curvature (Toloraiya et al., 2002; Liu et al., 2010; Duan et al., 2010), homogenous precipitation and phase formation (Bondarenko and Kablov, 2002; Liu et al., 2010; Reed, 2006, p.157; Karunaratne et al., 2001), equiaxed grain formation (Pollock et al., 1992; Dong et al., 2004; Liu et al., 2010), freckle formation (Reed, 2006, p.140; Pollock et al., 1992; Tin and Pollock, 2003) and pore formation (Bondarenko and Kablov, 2002; Orlov, 2008).

1.4.1 - Dendrite arm spacing λ (m)

The primary dendrite arm spacing is the main structural characteristic and since the result of refining it is improved tensile, creep, and fatigue properties, this becomes the primary reason for raising G_L (once G_L has surpassed the minimum value to prevent certain defect formation). λ has been shown in the literature to be proportional to the solidification range and $G_L^{-1/2}v^{-1/4}$ (Reed, 2006, p.144-147). Low gradient processing gives a large mushy zone (promoting defect formation), in which case secondary-order dendrite arms can form and overlap interdendrite channels, hindering the flow of the melt and reducing the homogeneity. Higher G_L reduces the size of the mushy zone, restricting the growth of the primary dendrite arms and suppressing the growth of the secondary order arms. This is represented by the shorter distance between the liquidus and solidus temperatures shown in the image on the right of figure 1.8. The resulting casting has a more uniform, finer-dendrite structure with smaller spacing between the dendrite arms (Kermanpur et al., 2000; Bondarenko and Kablov, 2002).

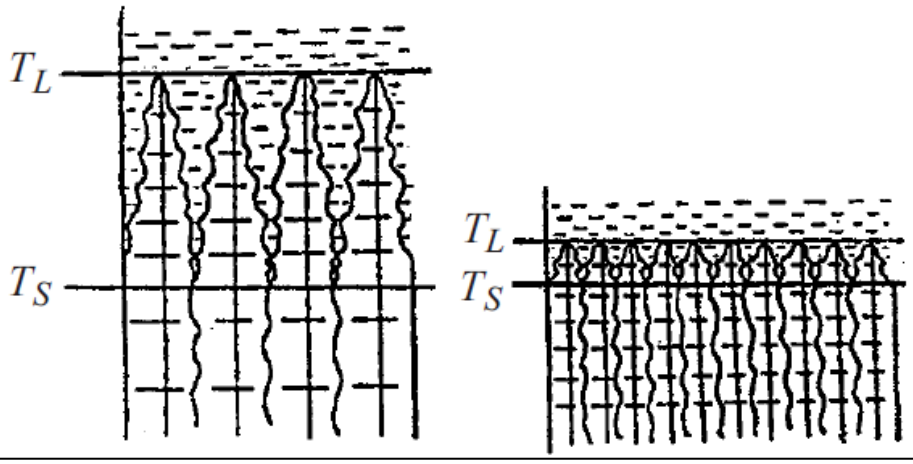

Fig. 1.8. Dendritic growth in DS between the solidus and liquidus temperatures. The larger scale of structure and size of mushy zone (left) G_L is undesirable compared to the more refined structure and smaller mushy zone given by a higher G_L (right) (Bondarenko and Kablov, 2002).

1.5 - Factors affecting the thermal gradient:

The work by Liu et al. (2010) highlights a number of factors that affect G_L. By analysing the heat transfer (based on the Fourier equation described by Fu and Wilcox (1980)), Liu and co-workers indicate the significance of a number of materials properties that affect the gradient. These are namely the conductivity (k), density (ρ), specific heat capacity (C_p) and the thermal diffusivity ($a=k_s/\rho_s.Cp$) (derived from the previous three). Also the sample diameter, certain control parameters such as heater temperatures, cooling medium, the withdrawal velocity and thermal baffles used can have an effect on G_L (Liu et al., 2010).

1.5.1 - Heat transfer coefficient:

A combined heat transfer coefficient (h) is a method of assessing the amount of heat transferred due to a specific process (Reed, 2006, p.136-139). It takes into account the different mechanisms of heat transfer e.g. in the HRS method heat transfer is influenced by four separate factors – conduction through the chill plate (h_C), conduction through the investment shell (h_{shell}), radiation across the gap at metal/shell interface (h_{gap}) and radiation from the shell to the vacuum chamber (h_R). Using the heat transfer coefficient described by Reed and values from other work (Konter et al., 2000; Elliot and Pollock, 2007) a mathematical analysis was done by Liu et al. (2010), highlighting why the LMC process gives beneficial gradients to the HRS process. Essentially this is due to h changing, as shown by the equations in figure 1.9 - for the LMC process h_R must be replaced with a heat transfer coefficient for cooling medium convection (h_f).

$$h_{\mathrm{HRS}} = \left(\frac{1}{h_{\mathrm{C}}} + \frac{1}{h_{\mathrm{gap}}} + \frac{1}{h_{\mathrm{shell}}} + \frac{1}{h_{\mathrm{R}}} \right)^{-1}$$

$$h_{\mathrm{LMC}} = \left(\frac{1}{h_{\mathrm{C}}} + \frac{1}{h_{\mathrm{gap}}} + \frac{1}{h_{\mathrm{shell}}} + \frac{1}{h_{\mathrm{f}}} \right)^{-1}$$

Fig.1.9. Heat transfer coefficients for the HRS and LMC processes (Liu et al., 2010)

The literature gives nominal values for the two processes above, finding that h_{HRS}=71 $Wm^{-2}K^{-1}$ and h_{LMC}=110 $Wm^{-2}K^{-1}$ (Liu et al., 2010), suggesting the LMC heat transfer coefficient for contribution to G_L is around 55% higher than the HRS process. Each value is subject to change however, depending on the specific casting dimensions. Liu's analysis is reinforced by Elliot et al. (2004) finding that values for G_L in the LMC process were approximately double that of the conventional Bridgman process (for 10mm thick sections at withdrawal rates up to 6.8mm/min).

With higher heat transfer coefficients (h_{HRS} and h_{LMC}), greater thermal gradients can be achieved. The ceramic moulds and the gap between them and the casting confine heat transfer causing G_L to reduce (Liu et al., 2010). These gap and shell contributions however cannot be altered significantly without removal of the ceramic mould. Focusing on the HRS process then, to raise G_L the h values for radiation interactions between the ceramic shell and furnace (h_R) and the conduction down the casting (h_C) need to be optimised. The heat transfer coefficient for each is given by the equations in figure 1.10:

$$h_R = \frac{\sigma(\varepsilon T^4 - \alpha T_0^4)}{T - T_0} \qquad h_C = \frac{\kappa_s}{X}$$

Fig.1.10. Heat transfer coefficients for radiation and conduction heat transfer processes (Reed, 2006, p.135).

h_R is derived from the Stefan Boltzman law that describes the heat transfer due to the difference in emission between one surface and absorption by the other, divided by the temperature difference between them. This equation introduces some important properties – the Stefan Boltzman constant (σ=5.67x10^{-8} W/m^{2}K^4), emissivity (ε) and absorptivity (α). h_C is found from the conductivity of the solidified alloy (k_s) , divided by the distance of solidified ingot (X) (X is proportional to the change in temperature). Reed (2006, p.135) gives values for these where initially h_C=1600 Wm^{-2}K^{-1} and h_R=120 Wm^{-2}K^{-1}. These give an indication of how much more contribution conduction has at the beginning of casting. However after a certain distance has solidified the h_C and h_R values become equal, beyond which the majority of the casting depends on radiative cooling. In addition for SX crystals produced with a spiral grain selector the conduction effect to the chill plate is reduced due to the small cross section of the spiral.

Therefore the majority of the casting is effectively cooled by radiation, which can be explained as follows: h_{HRS} is maximised when h_C, h_{gap}, h_{shell} and h_R are minimised but since the gap and shell terms are defined by the presence of the mould and the conduction invariably reduces as casting continues, focusing on the radiation is the most promising method for improving G_L. Figure 1.11 shows values for the HRS process given

by Liu et al. (2010), giving an idea of the magnitude of the different heat transfer contributions. Again these values are dependent on the size of the casting and alloy properties, explaining why they differ from the values given by Reed.

$$h_{\mathrm{HRS}} = \left(\frac{1}{1500} + \frac{1}{230} + \frac{1}{250} + \frac{1}{200} \right)^{-1} = 71\,\mathrm{W\,m^{-2}\,K^{-1}}$$

Fig. 1.11. Values of h for the HRS process from (Liu et al., 2010). Note h_C and h_R here are slightly different to Reed's values as they depend on casting dimensions and alloy properties.

Liu et al. (2010) also found that latent heat has no notable influence on G_L. Growth rate does however where increasing growth rate causes G_L to decrease. The paper then discusses how superheating of the melt (in particular just above the s/l interface), intensifying the cooling process and the use of small samples and effective radiation barriers are all advantageous for raising the gradient. This leads onto the work of this project, which will attempt to investigate some of these factors further, and others that might allow improved G_L.

1.6 - Typical thermal gradients currently achieved:

The Bridgman technique creates G_L via radiative heating in the hot zone and cooling of the casting by radiation to the furnace in the cold zone. In analysing the heat transfer mathematically, (Reed, 2006, p.134) has shown that in theory a thermal gradient of around 7500 K/m could be achieved, but this is unrealistic as it is impossible to achieve no heat loss from the hot to cold zone. Typical gradients achieved commercially with the

Bridgman method are in the region of 1000-2000 K/m. Such gradients can only be matched with low rates of solidification and cooling and tend to promote the formation of structural defects (Bondarenko and Kablov, 2002).

The introduction of a water cooled copper chill plate in HRS allowed improvements on the basic Bridgman process, achieving G_L values around 3000-4000 K/m, giving cast microstructures of dendritic form where the primary dendrite arm spacing is in the region of 100-500 μm (Reed, 2006, p.127). Reed (2006, p.138) theoretically compares the LMC process with HRS and states that: '…the LMC process affords an increased thermal gradient of at least a factor of 3 and a growth velocity of at least factor 2 over the convention Bridgman method.'

Findings obtained in the Russian study by Bondarenko and Kablov (2002) concur with this, concluding that DS with the Bridgman method cannot provide further improved gradients on the solidification front since the heat removal via radiation is limited compared to conduction and convection. This study then went on to investigate a number of different methods in the 'UVNÉS series'. The findings can be briefly summarised as follows: the use of LMC exhibited a gradient of 8000 K/m (an increase consistent with Reed's calculations) and when combining LMC with double zone heaters, heat screens and an increased furnace operating temperature a gradient in the region of 20000-25000 K/m was achieved (Bondarenko and Kablov, 2002).

Methods for high gradient DS were also developed by Liu et al. (2010). Firstly high overheating of the melt combined with LMC (HGLMC) was found to give a gradient of 38000 K/m. Problems were found with this however to do with overheating of ceramic

moulds at temperatures over 1700°C but it was found these can be overcome by only superheating a small section of the casting, adjacent to the s/l interface. This zone intensified overheating with LMC (ZIOLMC) produced a massive thermal gradient of 80000 K/m. It should be noted these two values were achieved under experimental conditions at low withdrawal velocity and in commercial casting higher v would be used - however the ZIOLMC method still produced a gradient of 36000 K/m at a speed of 2.50×10^{-4} m/s – considerably higher than normal LMC values, and higher than the best gradient achieved in the UVNÉS series.

Liu et al. (2010) then discuss how ceramic moulds confine heat transfer and the development of a new method utilising electromagnetic confinement (EMCDS) of the molten sample, thus eliminating the need for ceramic moulds. Such a method therefore eliminates any effect on heat transfer the shell has so the h_{gap} and h_{shell} terms are eliminated from the heat transfer coefficient, as shown in figure 1.12.

$$h_{\mathrm{HRS1}} = \left(\frac{1}{h_{\mathrm{C}}} + \frac{1}{h_{\mathrm{R}}} \right)^{-1}$$

and

$$h_{\mathrm{LMC1}} = \left(\frac{1}{h_{\mathrm{C}}} + \frac{1}{h_{\mathrm{f}}} \right)^{-1}$$

Fig. 1.12. The heat transfer coefficients for HRS and LMC if ceramic moulds are successfully removed with EMCDS (Liu et al., 2010).

This gives potential for improved heat transfer, allowing higher G_L to be achieved. This method is still in the experimental stages however and some way from introduction

commercially. For example, it is unclear whether the loss of ceramic moulds would prevent hollow form blades with complex cooling channels to be produced, or if there is some way of replicating the cooling channels using electromagnetic confinement.

1.7 - Summary

Extensive work has been done in increasing the thermal gradient - the highest exhibited so far (at a commercial withdrawal speed of 2.50×10^{-4} m/s) is at 36000 K/m found by Liu et al. (2010). The use of localised intensified overheating of the melt, increased furnace operating temperature, improved cooling, effective radiation barriers and small sample diameter are all beneficial for increasing G_L. These higher gradients can allow more rapid solidification, but it is important to maintain some degree of control over the cooling rate – high cooling rates decrease the dendrite arm spacing, but excessive rates can lead to extreme curvatures of the solidification front, high radial temperature gradients, the growth of secondary dendrite branches and nucleation of crystal grains on the wall of the mould. High solidification rates also promote the formation of a non-equilibrium structure, eutectic phases in the first turn.

2.0 - AIMS:

High G_L on the solidification front is crucial for DS and the use of double-heater zones, heat screens and increasing working temperatures of the furnace all tie in with this project. Rapid heat loss by radiation in the cold zone leads to higher gradients being achieved but little can be done to improve this that has not already been investigated (with the use of water cooled walls/LMC etc.). There is however a lack of work investigating methods of retaining radiation in the hot zone and optimising G_L in this way.

It is already known that effective thermal baffle selection is important for G_L (Liu et al., 2010) but it is proposed that more effective selection of novel radiation barriers could potentially further optimise G_L. The thermal baffle is defined by others (Liu et al., 2010) as an isothermal material located between the hot and cold sections of the furnace to act as a barrier and prevent the thermal flux from transferring between them. In the case of a normal baffle however, in reality during casting the baffle is not necessarily isothermal (all at the same temperature) as some radiation absorption will mean a temperature gradient across the thickness of the baffle. Liu et al. (2010) also state that the baffle thickness has some effect, with thick baffles promoting a flat s/l interface but also reducing G_L (Liu et al., 2010). Graphite foil has a high emissivity and is not very reflective - until now there has been no work investigating reflective baffles in DS. Bondarenko and Kablov (2002) mention the use of water cooled circular screens to aid heating at the bottom of the furnace however it is unclear whether these are reflective or if they are to complement or replace the baffle. Effectively reflecting radiation back into the hot zone should improve heating of the mould and also minimise the temperature

gradient across the baffle hence minimising emission into the cold zone from the base of the baffle itself. With high reflectivity it should mean the high resistance to conduction found with graphite baffles is unnecessary as although metals have high conduction, the low emissivity should mean the majority of incident radiation is reflected and not absorbed by the baffle, so cannot be conducted through it to the cold zone.

The aims of this project are to investigate the use of reflective baffles both experimentally and numerically as coatings/replacement of graphite foil to control radiation and heat transfer in the DS furnace. The development of a computer model to accurately model the heat transfer in the furnace will allow the potential effect of new baffle materials on the thermal gradient to be assessed before selecting appropriate candidates to be trialled in the HRS furnace at Birmingham. If sufficient improvement is seen then the current work will propose a design for a new type of baffle and cast a superalloy component under actual turbine blade casting conditions to assess the benefits in microstructure given by the improved G_L.

Since the furnace at Birmingham uses a HRS Bridgman system, improvements on the high experimental values of G_L found by Bondarenko and Kablov (2002) and Liu et al. (2010) will not be achieved. However should the novel baffles prove to be effective at raising G_L in the HRS system, it may be possible to apply the theory to more if not all variations on the DS process. Even in the case of a floating baffle for LMC, for example, if the current work proves effective it may be possible to introduce a highly reflective baffle above the floating baffle, blocking the majority of radiation then allowing the floating baffle to block any still getting through.

3.0 – HEAT TRANSFER IN THE FURNACE:

The use of an analytical model was vital to fully understand the heat transfer and hence the factors that affect G_L on the solidification front. The casting was modelled as an infinite cylindrical rod moving at a uniform rate v, so the heat flow follows the Fourier equation (Fu and Wilcox, 1980). The Fourier law for the conditions of quasi-stationary heat flux states that under such conditions the temperature on the solidification front increases in proportion to the density of the heat flux through the side walls of the mould. The steady-state balance that exists between the rate of heat extraction by conduction along the casting in the axial direction and the rate of transverse heat loss by radiation through the curved cylindrical surfaces was analysed by Reed (2006, p.131-135). In reality, at the beginning of casting, this steady state balance has yet to be reached.

This relationship was important since the baffle is a radiation barrier and the primary aim was to maximise the radiation retained in the hot zone, thus minimising heat transferred to the cold zone. If the heat transfer by conduction down the casting to the chill plate was found to have much greater effect than the radiation from the mould surface then optimising the baffle could have only made limited difference. As described by the heat transfer coefficients h_C and h_R, at the beginning of DS the primary contribution to heat loss is through conduction to the chill plate, which decreases as the length of solidified casting increases. Thereafter, heat loss by radiation dominates, which is aided by the small cross section (of both the casting and the spiral grain selector) and the substantial surface area of the mould (Reed, 2006, p.135).

3.1 - Heat transfer Theory:

As mentioned, the four separate mechanisms of heat transfer acting simultaneously on the casting in HRS are: conduction through the chill plate, conduction through the investment shell, radiation across the gap at metal/shell interface and radiation from the shell to the vacuum chamber (Liu et al., 2010). Radial heat conduction through the investment shell and radiation across the gap between the shell and casting could not be altered in the furnace, so while it was important to note these processes were occurring, for the purpose of the model it was much more important to consider the vertical thermal gradient. Therefore a 1-D model was developed to analyse this due to the contributions from radiation, conduction and withdrawal.

3.1.1 - Radiation:

Thermal radiation is defined as energy emitted by matter in the form of photons/electromagnetic waves that does not require the presence of any material medium. Radiation can be emitted, absorbed, reflected and transmitted (by semi-transparent materials). It can be viewed as a surface phenomenon in most solids and liquids (but not gases and semi-transparent solids) and accordingly the radiation emitted originates from the molecules within roughly 1μm of the surface. Since the materials in the DS furnace are opaque the interaction of radiation was treated as a surface phenomenon. Radiation has a somewhat complex description in that it exhibits two defining characteristic features – its magnitude varies with wavelength, defined by a spectral distribution (i.e. the radiation emitted encompasses a range of wavelengths) and

a directional distribution (a surface may emit preferentially in certain directions). These are dependent on the temperatures and materials involved (Incropera, 2007, p.725-726).

3.1.2 - Radiation exchange between diffuse grey surfaces:

When considering the radiation exchange between the bodies in the furnace grey surface behaviour was assumed. With the hot and cold zones approximated as large isothermal enclosures, small bodies confined within them (such as the casting) would have negligible influence on the radiation field (Incropera, 2007, p.762). The furnace is the dominant radiation source and the bodies in it are relatively small, so the furnace temperature controls the baffle temperature and both the furnace and baffle temperatures control the mould temperature. To model this, the contributions of the different surfaces of the furnace to the mould temperature were analysed with the use of view factors (Incropera, 2007, p.762-766). In the cold zone, the conditions for radiation are exactly the same as the hot zone except the casting is hotter than its surrounding surfaces so heat is lost to them, rather than being gained from the furnace.

Under such conditions, when the furnace has reached its set temperature steady state can be assumed and the thermal baffle (and for that matter all other 'small' bodies in the furnace) can be approximated as grey surfaces being diffusely irradiated, where the emission of the furnace is proportional to T^4. Derived from the Stefan-Boltzman law, (Incropera, 2007, p.738) the net rate of radiation heat transfer per unit area for a small grey surface A_1 irradiated by a grey body A_2 (see figure 3.1) is given by:

$$q_{RAD} = dA_1\, dA_2\, \varepsilon_1\, \varepsilon_2\, \sigma\, (T_2^4 - T_1^4)\, (\cos\theta_1 \cos\theta_2 / S^2) \qquad (W) \qquad [1]$$

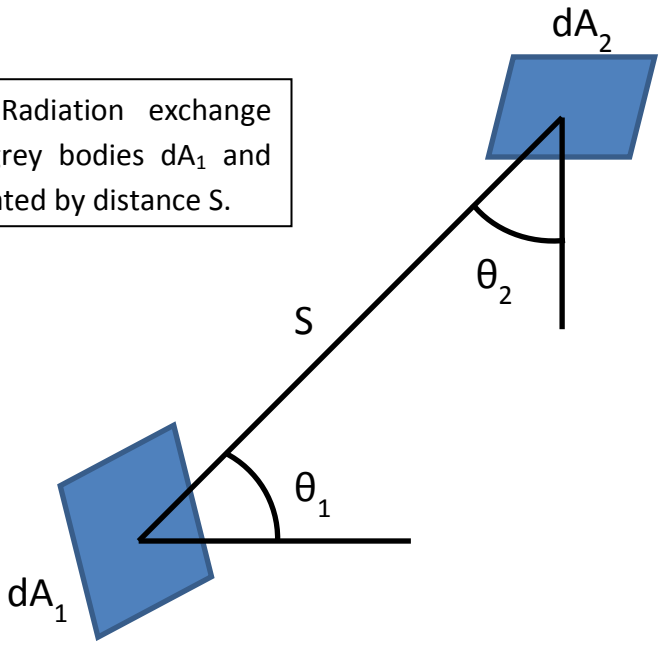

Fig. 3.1. Radiation exchange between grey bodies dA_1 and dA_2, separated by distance S.

3.1.3 - View factors (F_n):

The inclusion of view factors involved taking the geometries of the furnace surfaces and internal bodies into account. A surface may emit diffusely but geometrical factors can prevent a body from 'seeing' all of that radiation. View factors were used to calculate the portion of radiative energy leaving one surface that can be intercepted by another, due to the physical shape and orientation of the surfaces. The view factor is a coefficient for a specific set of geometries e.g. from the point of view of the mould, the top of the furnace had a different view factor to the side of the furnace. The view factor equals the fraction of the field of view from the point dA_1 filled by a part of the furnace, taking a value between 0 and 1, where if F_n=1 point dA_1'sees' only radiation from that emitting surface (Incropera, 2007, p.812-815). In modelling the furnace, seven main view factors were calculated to represent the radiative exchange between the mould and all the relevant surfaces. These are shown in figure 3.2 – in the term F_n, n is an integer, taking values from 1 to 7 depending on which view factor is being described.

In this work, for every point dA_1 on the mould, ($dA_2 \cos\theta_1 \cos\theta_2 / S^2$) was integrated for each surface in the furnace, so the view factor was given by:

$$F_n = \Sigma\, dA_2 \cos\theta_1 \cos\theta_2 / S^2 \qquad [2]$$

The heat transfer due to radiation then became:

$$q_{RAD} = dA_1 F_n \varepsilon_1 \varepsilon_n \sigma (T_n^4 - T_1^4) \quad (W) \qquad [3]$$

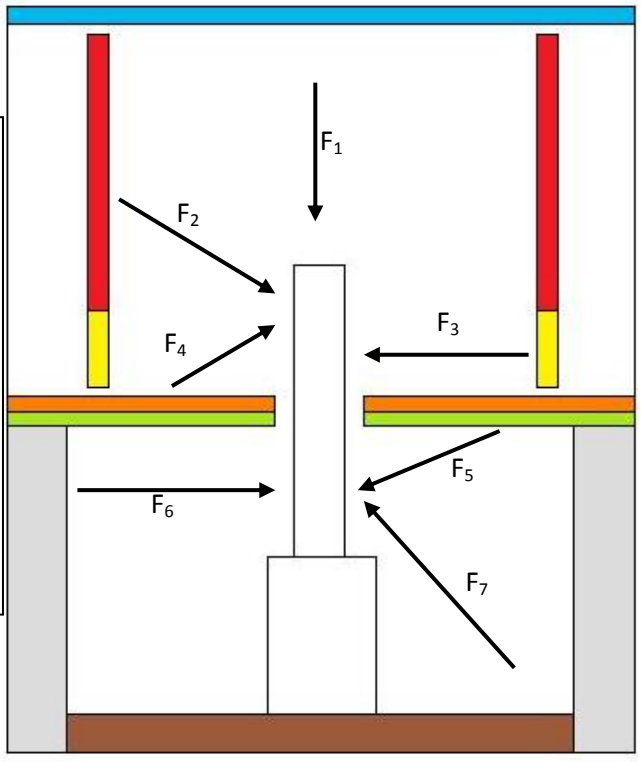

Fig 3.2. View factors that were modelled in the furnace. The seven view factors:

- F_1 - the top of the furnace
- F_2 - heater upper
- F_3 - heater lower
- F_4 - baffle top
- F_5 - baffle bottom
- F_6 - cooling zone side walls
- F_7 - bottom of furnace.

Different colours are used to clearly illustrate each view factor.

All the geometrical factors were included within the term F_n. These view factors were calculated using a code written in MATLAB by another student, Abhay Soorya (Soorya, 2010). The model also included the vertical conduction along the axial direction of the casting. The heat flux for conduction was given by a basic conduction equation:

$$q_{CON} = k .dA. (T_1 - T_2) / L \qquad (W) \qquad [4] \qquad \text{(Incropera, 2007, p.59)}$$

Where A is the cross-sectional area of the casting (m^2), k is the thermal conductivity (W/m/K) and L is the distance the heat is conducted through (m). Since it was impossible to alter h_{gap} and h_{shell} short of utilising some kind of electromagnetic confinement method as described by Liu et al. (2010) the focus of this project was on the relationship between equations [3] and [4].

At steady state radiation incident on the ceramic mould is not just from the graphite resistance heaters but from a combination of emission and reflection from all parts of the hot zone. This radiation was modelled as exchange between diffuse grey surfaces meaning (ε=α) could be approximated (from Kirschoff's law) and since they were treated as 'grey', ε and α were independent of wavelength (Incropera, 2007, p.762-766). Radiation is incident directly onto the thermal baffle from the heaters and other parts of the furnace. Therefore it was anticipated that if the baffle material selected was of low emissivity and had a highly polished surface finish then the amount of incident radiation absorbed by it would be minimised (and more reflected back to heat the mould). Also since minimal radiation would be absorbed, the amount of radiation that could be emitted from the base of the baffle into the cold zone would also be minimised. Due to these mechanisms, it was hoped by replacing current baffle materials with much lower emissivity materials an improvement in G_L would be exhibited.

3.2 – Emissivity (ε)

Emissivity is the ability for radiant heat to leave the surface of an object. It is a property that is independent of density, mass or thickness but is dependent upon the material

selected, its surface finish and temperature (Incropera, 2007, p.744). ε takes values between 0 and 1 and describes how close a real material's behaviour is to that of a blackbody of the same material. From Kirschoff's law for a body at thermal equilibrium, emissivity ε = absorptivity α (Incropera, 2007, p.762-763). Table 3.1 shows possible candidate materials.

Table 3.1: Candidate baffle materials

	Graphite (Current baffle)	***Polished gold***	***Polished copper***	***Polished Aluminium***	***Platinum***
Melting point T_m (^oC)	3650	1064	1084	660	1768
Emissivity ε	0.70-0.90	0.015-0.03	0.02-0.05	0.01-0.10	0.01-0.09
References	(Elliot and Pollock, 2007; Kostanovskii et al., 2005)	(Giulietti and Lucchesi, 1981; Brandes and Brooke, 1992, p.17.10)	(Window and Harding, 1981; Giulietti and Lucchesi, 1981; Brandes and Brooke, 1992, p.17.10)	(Giulietti and Lucchesi, 1981; Reynolds, 1961; (Brandes and Brooke, 1992, p.17.10)	(Brandes and Brooke, 1992, p.17.10; Deemyad and Silvera, 2008; Bradley and Entwistle, 1961)

Table 3.1. All values for Tm taken from Brandes and Brooke (1992, p.14-1) apart from graphite foil – data courtesy of Lowden metals Ltd.

Table 3.1 gives a range of values for emissivity to highlight the property dependence on material purity, surface finish and temperature. These are nominal values that would be considerably different, for example, with a rough surface. Generally with metals an increase in temperature gives an increase in emissivity, due to increased resistivity. This is however dependent also on wavelength, as in the infra-red region this is generally true

but not necessarily in the visible and ultraviolet regions (Brandes and Brooke, 1992, p.17.1–17.4).

Whilst the high resistance to conduction perpendicular to the surface is beneficial with graphite foil baffles (Elsden, 4 March 2010) (graphite foil data courtesy of Lowden Metals Ltd., Halesowen), it will still absorb a relatively large portion of the radiation incident upon it. This may take a while to conduct through the graphite foil but nevertheless some of it will be conducted through and may then be free to emit into the cold zone. It was proposed that replacing graphite foil with a low emissivity baffle would improve the reflection of radiation incident upon it back into the hot zone, which should lead to improved G_L.

All the metals listed in table 3.1 have lower emissivity than graphite so they all had potential to be used in its place, however other properties eliminated some of them as candidates. Aluminium foil would have been least expensive but its melting point is much too low. In terms of both temperature capability and emissivity, platinum seemed the ideal choice for a novel reflective baffle - its melting point is 1768^{o}C (higher than the highest operating temperature used in the furnace at Birmingham). Platinum is very expensive however and at least for initial experimentation the cost could not be justified. Highly polished copper and gold however both have relatively low emissivities too and cost less than platinum. Although their melting point is not as high, these were selected as the two materials for initial testing.

4.0 – MODELLING

4.1 - Development of the model:

A model was developed with MATLAB and GNU Octave software incorporating all relevant variables, allowing furnace geometries, casting geometries, materials properties, baffle position, component temperatures, withdrawal velocity and the time step to be altered if desired.

To represent a real size of casting, it was modelled as a finite cylinder split into small cells with a position vector assigned along the vertical axis of the furnace, allowing the casting to be monitored as it was withdrawn through the furnace. When running, first the model calculated all the view factors (that were shown in figure 3.2). These were i) the top of the furnace, ii) heater upper, iii) heater lower, iv) baffle top, v) baffle bottom, vi) cooling zone side walls and vii) base/water chill plate. Figure 4.1 shows an example of how the model dealt with the temperature changes on a single cell.

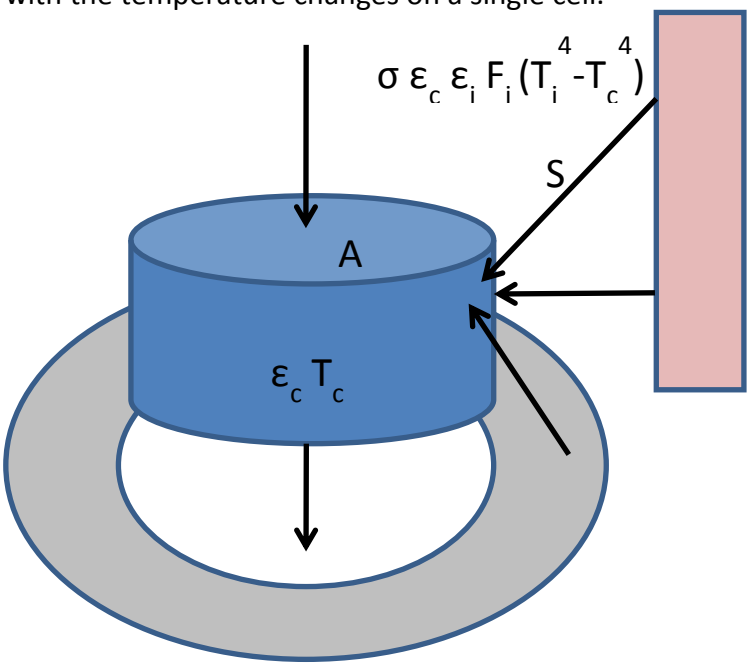

Fig.4.1. A simplified representation of the heat transfer on one cell in the model.

On each cell, for the given view factors the model ran loop calculations for the total power in and out of that cell, taking into account radiation and conduction. Each cell was assigned an initial temperature then the model calculated the temperature change due to heat transfer after a short time interval dt. It repeated this until enough time had passed that the cell temperatures should be moved down by one cell to simulate the withdrawal. This was repeated until the temperatures from one withdrawal step to the next were within 0.001^{o}C. The bottom cell of the casting was not force cooled to represent the chill plate - this was done to simulate the presence of the small diameter (in comparison to the mould) spiral grain selector which in reality diminishes the conduction effect, adding to the dominance of radiation seen with 'tall' castings.

4.2 - View factors:

The view factors from the furnace walls were treated normally, but to simulate the use of a shiny baffle the model treated the baffle view factors differently. As the new baffles to be simulated were very reflective, the model was told to calculate the sum of the radiation emitted from the baffle itself, plus the reflection of radiation from the other view factors that could be 'seen' by the relevant baffle surface. As a crude example to explain the principle, if the model was analysing the radiosity from the top of the baffle (F_4) incident on area dA_1 on the mould, it calculates it as the sum of F_4 plus the reflected portion of radiation from the view factor for the heaters (F_2+F_3), so F_4 in actuality = F_4+R(F_2+F_3) where R is a coefficient representing how much of the heater radiation is reflected, given by: $R = 1-\varepsilon_{baffle}$ (lower baffle emissivity mean higher R).

4.3 - Modelling approach:

The approach was to set all the parameters to represent the furnace in real life as closely as possible - furnace geometries, casting geometries, material properties, temperatures etc. The model defined all variables then calculated how the temperature of the casting changed due to the heat transfer mechanisms occurring in the furnace. It took into account the materials properties, heat transfer equations and withdrawal of the casting into the cold zone. It then plotted graphs for a) temperature vs. position and b) thermal gradient vs. position and calculated the thermal gradient across the solidification range by finding the liquidus and solidus cells.

The conduction through the investment shell and radiation across the gap at metal/shell interface were not included in the model to maximise its speed. If included it would have represented real life more accurately, but the purpose of the model was a tool to identify trends seen in factors affecting the G_L. The model was required to validate the theory about low emissivity baffles so any unnecessary practical work could be avoided; hence extensive work was put in to give a model showing realistic trends.

The withdrawal velocity, number of cells and the baffle position (central) were kept at a constant and so were furnace geometries apart from heater split height and baffle gap. The heat transfer mechanisms (and hence equations used in the model) are process dependent so were also kept constant to simulate HRS. Having said this, however, the model was versatile enough to be relatively easily modified to look at such factors in more detail, e.g. to model the LMC process would simply have required the

inclusion of suitable convection cooling equations and the materials properties of the cooling medium.

The materials properties used were for CMSX-4 alloy, obtained from Matsushita et al. (2009) and are shown in table 4.1.

Table 4.1 – Alloy properties used during modelling:

Component	***ρ (kg/m^3)***	***C_P (J/kg/K)***	***k (W/m/K)***	***$T_{Solidus}$ (K)***	***$T_{Liquidus}$ (K)***	***ε***
CMSX-4 (at 1500K)	7900	1000	25	1594	1654	0.70
Source	(Matsushita et al., 2009)					Alaruri et al., 1998)

For the other parts of the furnace, emissivities and temperatures were assigned (see table 4.2) and then kept constant apart from the baffle emissivity (unless otherwise stated subsequently). Since diffuse radiation had been assumed, all insulating parts of the furnace were given ε=1 (in reality, all the furnace materials that make up heaters or insulating surfaces have high emissivity anyway).

Table 4.2 – Thermophysical properties used in modelling:

Component	Ceramic mould	Heaters and furnace chamber walls	Copper baffle (highly polished)	Graphite foil baffle
Emissivity ε	0.7	1	0.05	0.9
Source	(Elliot and Pollock, 2007)	Approximated to represent diffuse grey surfaces	(Giulietti and Lucchesi, 1981)	(Kostanovskii et al., 2005)
Conductivity k (W/m/K)	2.5	/	397	2
Source	(Elliot and Pollock, 2007)	/	(Brandes and Brooke, 1992, p.14-1)	(Elsden, 4 March 2010)

Variables used:

Unless otherwise stated, all test runs of the model were done modelling a cylindrical casting of CMSX-4 alloy of height 0.2m and radius 0.01m, with the following values:

Other variables:

- Withdrawal velocity $v=6.5\times10^{-5}$ m/s (a typical withdrawal velocity used in casting).
- Time step dt=0.025 s.
- Cell height dz=0.001 m.
- Casting radius r=0.01 m.
- Casting-baffle clearance gap=3 mm.
- Stefan Boltzman constant $\sigma=5.67\times10^{-8}$ W/m^2K^4.

Temperatures:

- Top of furnace was estimated to be slightly lower than top heater temperature – set to 1200^{o}C at heater temperatures of 1300^{o}C.
- All runs with a graphite foil baffle used an optimiser calculation to estimate the temperatures across a 2mm graphite baffle. Runs with a copper baffle had baffle temperatures set to 100^{o}C to simulate water cooling (as is the case with the base chill plate).
- The walls of the cold zone were also estimated to be 100^{o}C.

4.4 – Modelling results:

A modified version of the code was run to optimise the heater to give the best G_L, with the condition that the mould temperature did not exceed 1670^{o}C (the maximum practical temperature the ceramic moulds are taken to). The current graphite heater in the Birmingham furnace is a single heater, however it was important to investigate theoretically using a two-part split heater to model superheating above the baffle. This was achieved by looping the model with an optimiser method until the best G_L was achieved from varying the heater split height and temperatures (for both a graphite and copper baffle).

This was repeated for a single part heater, to allow the potential improvement over the current set up to be analysed. The optimum temperatures found were then kept constant for subsequent simulations. The findings for G_L with the best heater parameters for a split heater are shown in table 4.3.

Table 4.3: Split heater optimised

Split height (cm)	*Top heater temp. (K)*	*Bottom heater temp. (K)*	*G_L (K/m)*	*Max temp. on mould (K)*	*Baffle material*
6	1300.00	1955.77	24857.11	1669.99	Graphite
2	1302.86	1991.77	30169.61	1660.36	Copper

The results indicated the split height required was smaller for a reflective baffle, suggesting reflection off the baffle aids heating of the mould, meaning a smaller portion of the heating elements require superheating (minimising this is desirable to avoid

degradation of the moulds over 1670^{o}C). The gradients found however were much higher than values normally seen for the HRS process. This may be explained as follows - it can be argued that with perfect heaters of ε=1 and no radial resistance to heat transfer included (from the presence of the mould), these results represent the 'best-case scenario' in terms of heat transfer in the furnace. For a more realistic simulation, the 'worst-case' also had to be considered. This occurs when heat transfers by radiation from the metal casting to the mould and conduction through the mould. Despite the model not including these radial heat transfer equations, the contribution of these effects was simulated by considering the combined emissivity of the alloy in the casting and mould. With ε_{Mould}=0.7 (Elliot and Pollock, 2007) and ε_{Metal}=0.7 (Alaruri et al., 1998), the combined emissivity was 0.54, using $\varepsilon_{combined} = 1/(1/\varepsilon_1+1/\varepsilon_2-1)$ (Incropera, 2007, p.833). This gave the combined emissivity for radiation exchange between parallel plates - strictly speaking the mould and metal are not parallel plates but rather concentric cylinders, but the difference in behaviour between these is small compared to the uncertainty in materials emissivities.

The 'mould outer emissivity' (NB. originally 0.7 - the value in table 4.2; not the same as ε_{Mould} mentioned above) was multiplied by this combined metal to mould emissivity as an approximation, which gave a new mould outer ε of 0.38. It was also perhaps unrealistic to assume the heaters and furnace surfaces had perfect emissivity. By using ε_{heater}=0.8 (Elliot and Pollock, 2007) and 'outer' ε_{mould}=0.38 in the model, more realistic G_L values were expected hence these values along with the optimum heater

parameters were then used for all subsequent simulations. Table 4.4 shows the thermal gradients found when re-running the simulations in table 4.3.

Table 4.4 (Split heater optimised - mould and heater emissivities revised):

Split height (cm)	*Top heater temp. (K)*	*Bottom heater temp. (K)*	*G_L (K/m)*	*Baffle material*
6	1300.00	1955.77	15370.67	Graphite
2	1302.86	1991.77	19040.98	Copper

The values for G_L (shown in table 4.4) were still higher than would be expected in a real life HRS process but they were much closer than the values originally obtained. The same was done to find the optimum temperature for a single part heater, shown in table 4.5. This allowed a comparison to be made with the thermal gradients achieved with the current setup and assess the potential for improvement.

Table 4.5 (Single heater - mould and heater emissivities revised)

Heater temp. (K)	*G_L (K/m)*	*Max temp. on mould (K)*	*Baffle material*
1681.15	14597.19	1662.13	Graphite
1676.87	18218.12	1669.99	Copper

In table 4.5 it is surprising that the graphite optimal result gave the best G_L at a max mould temperature of 1662^{o}C, not 1670^{o}C. This was perhaps due to the graphite baffle heating up as the heater temperature rose, or perhaps a slight issue in how the gradient was calculated in the model - done by finding the liquidus and solidus cells, meaning the number of cells in-between could jump, which might have affected the gradient in a way that's not smooth. Alternatively it may have been a result of the position of the solidus

and liquidus cells within the furnace with respect to the baffle position. If either of these statements is true, it does not make the trends shown in subsequent simulations invalid, as the effect on the values seen would only be small.

Despite the gradients being higher than expected the results showed the correct trends. The model indicated a clear potential for raising G_L with lower emissivity baffles. The G_L values suggest the use of a water cooled copper baffle could give improvements of around 25% over graphite (with both a split heater and single heater). Also, the use of an optimised split heater could give improvements of about 5% in G_L over a single heater for both baffle types.

The model was then used to investigate the casting size (height and radius) and baffle gap's (distance between baffle and mould surface) effect on G_L and to compare the trends shown by the model with trends in the literature. Altering these geometries required the calculation of new sets of view factors. These were all simulated with a water cooled copper baffle, as repeating every run with both baffle types was pointless. The results for all simulations are shown in table 4.6 (the first four runs show the results from table 4.4 and 4.5 for easy comparison).

Table 4.6 – All modelling results:

Run	*G_L (K/m)*	*Variables*	*Baffle material*	*Heater type*
1	15370.67	Corrected emissivities; best heater temps & split height; baffle material.	Graphite	Split heater
2	19040.98	Corrected emissivities; best heater temps & split height; baffle material.	Copper	Split heater
3	14597.18	Corrected emissivities; best heater temp; baffle material.	Graphite	Single heater
4	18218.12	Corrected emissivities; best heater temp; baffle material.	Copper	Single heater
5	11959.80	Casting radius doubled to r=0.02m, baffle inner = 0.023m. (original height + baffle gap)	Copper	Split heater
6	20092.25	Casting height doubled to cell height dz=0.002m (original radius + baffle gap)	Copper	Split heater
7	18463.19	Baffle gap doubled to 6mm (original casting size)	Copper	Split heater

Table 4.6. Shows the results from all simulations (the first four are those discussed for the optimum heater parameters for both baffles and heater set-ups, shown in table 4.4 and 4.5). For all other variables changed (runs 5-7), comparison with run 2 indicates the effect they individually have on G_L in the model (since they were all done with a split heater and copper baffle).

Figures 4.2 and 4.3 show the graphs plotted by the model for runs 2 and 3 in table 4.6 respectively – note although there is a bigger difference in G_L between runs 3 and 6 with the increased casting height, in reality the casting height is chosen depending on the purpose, not optimising G_L. Therefore the comparison of runs 2 and 3 shows the potential improvement over the current setup at Birmingham. Only the graphs for these runs have been included as they are most relevant.

Figure 4.2: Run 2 – All parameters optimised:

a) Temperature v Position

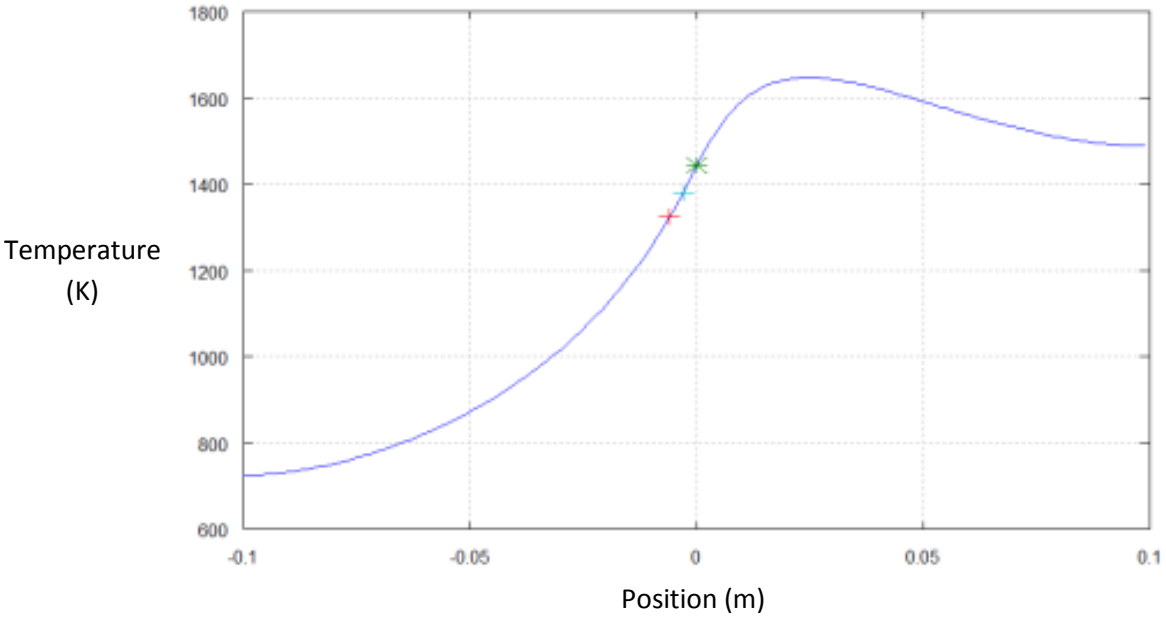

b) Thermal gradient v Position

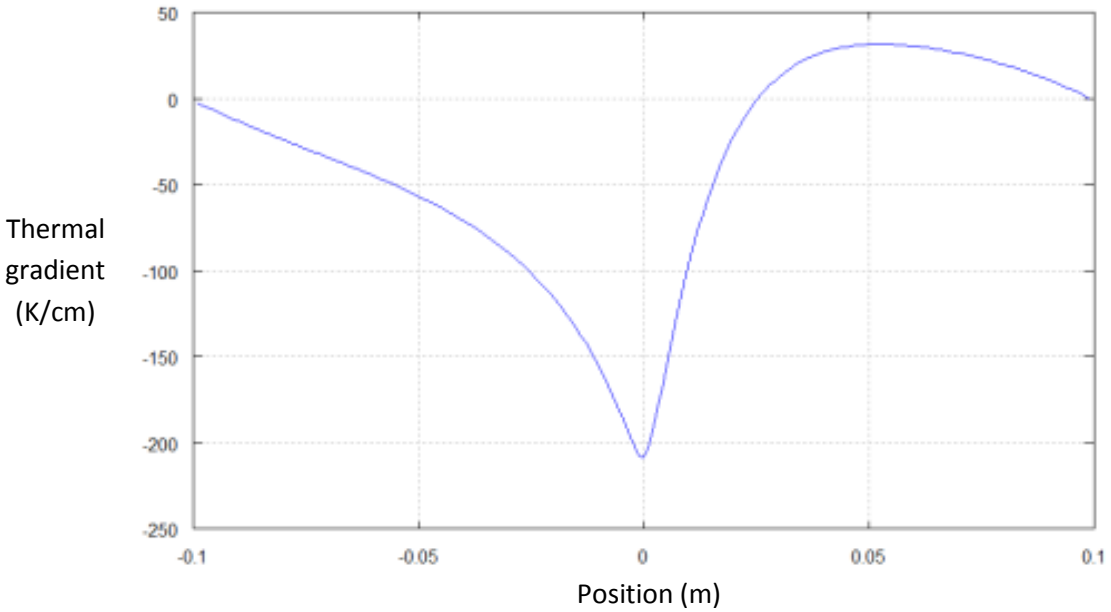

Fig.4.2. Modelling graphs for all optimised parameters - G_L=19040.98 K/m (water cooled copper baffle, split heater at optimal temperatures and minimal baffle gap), showing:

a) Temperature v position
b) Thermal gradient v position

Figure 4.3: Run 3 – Current setup at Birmingham:

a) Temperature v Position

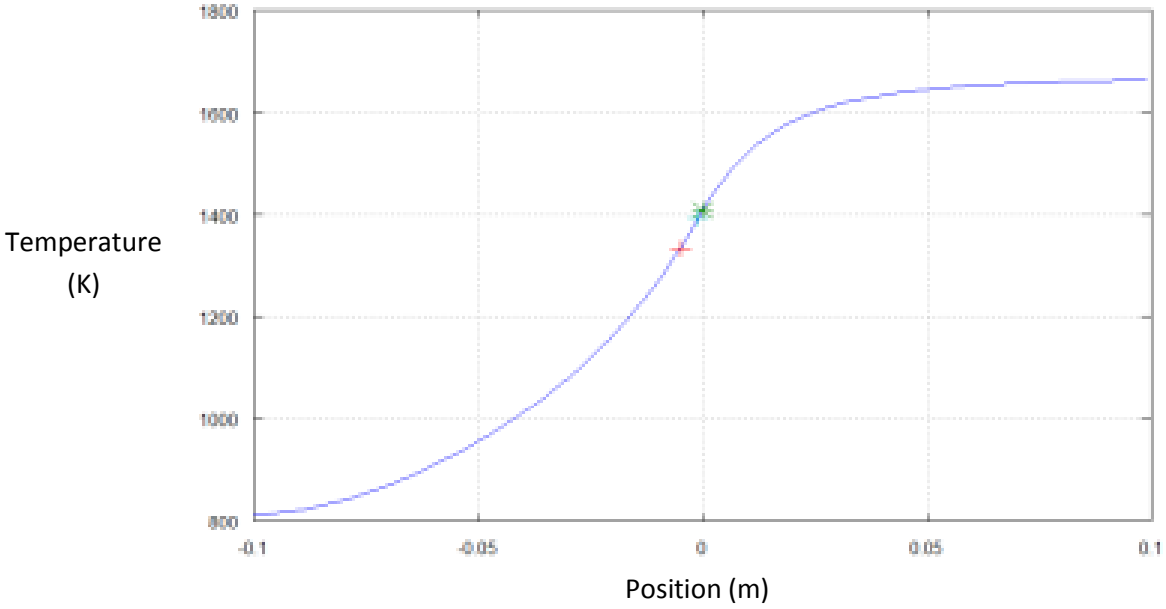

b) Thermal gradient v Position

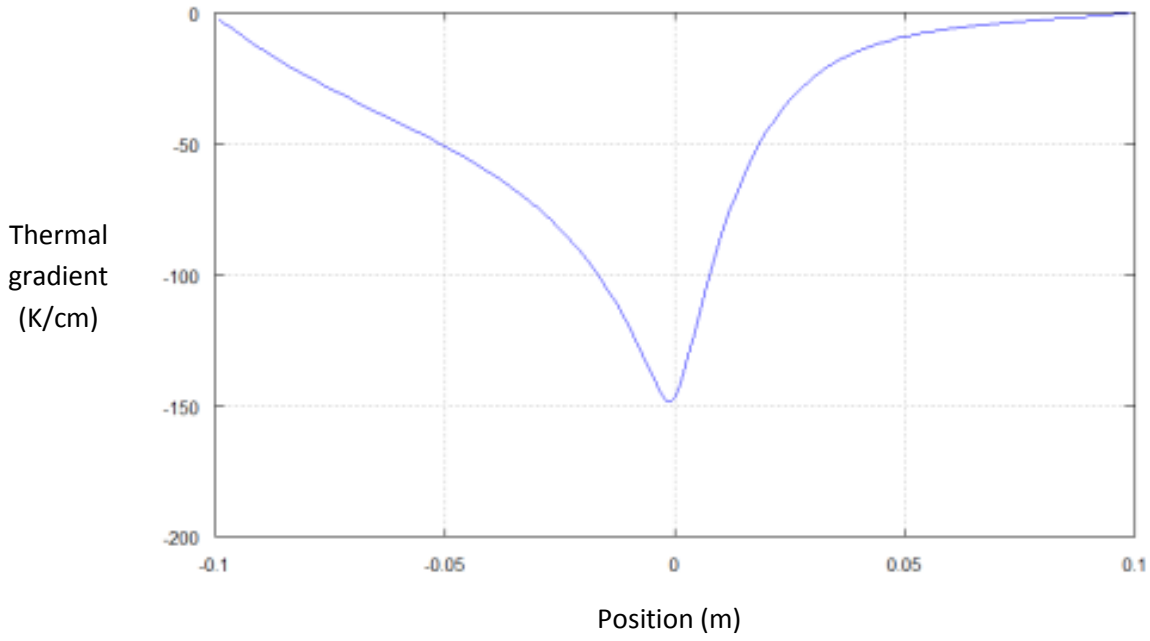

Fig.4.3. Modelling graphs for standard parameters - G_L=14597.18 K/m (uncooled graphite foil baffle, single heater at optimal temperature and minimal baffle gap), showing:

a) Temperature v position
b) Thermal gradient v position

The model suggested doubling casting radius had the effect of lowering G_L considerably by around 37%. This was as expected as it is already known the thermal gradient should decrease with increasing casting radius due to the enhanced conduction.

Doubling casting height exhibited a slight increase in G_L of around 5%. Again this was expected since the radius was constant so the conduction effect would be the same, but increased casting height means more surface area for heating and cooling by radiation.

When doubling the baffle gap a slight decrease in G_L was found. This result also acted to validate the trends found by the model because despite the difference only being small, it is known from the literature that minimising the baffle gap is important for maximising G_L. It is perhaps also correct to only expect a slight difference in G_L here anyway because the model considered a cylindrical casting of constant cross-section. This parameter is however more important in casting actual turbine blades where the profile is complex. Particularly in the case of large radius castings the baffle gap is important to ensure very strict control of G_L. No further simulations were done with a smaller baffle gap than 3mm since in reality the investment shell is not a perfect cylinder, so a uniform gap cannot be achieved consistently throughout casting.

Investigating these other variables proved to be crucial to analysing the potential for improving G_L. For example, optimising the heater temperatures and split height was critical as the different baffles exhibited different optimal split heights. Had these simply been guessed and kept constant, the results may not have showed the trends as accurately e.g. if the chosen split height was closer to the optimum split height for copper

than for graphite. Thus the effect of the baffle on G_L could be more accurately predicted using the model this way. It would require practical experimentation to investigate whether in the actual furnace 2cm would be the optimal split height for a copper baffle but the model did show that reflective baffles allow minimal superheating.

To summarise the modelling confirmed findings from the literature that tall castings with low radius and a minimal baffle gap are beneficial for raising G_L. It also showed localised superheating is better than a single heater and by utilising water cooled, low emissivity, reflective copper baffles a potential increase in G_L of around 25% may be found over traditional graphite foil baffles. Combining all of these factors, the model suggested a potential increase in G_L of around 30% over that obtained in a DS furnace like the one used at Birmingham (the difference between G_L in runs 2 and 3 in table 4.6 where run 3 represents the setup currently used at Birmingham).

4.5 - Sensitivity study:

A sensitivity study was done to ensure the model was calculating G_L to an accurate degree. This involved varying the time step and the cell size used in the model – accurate modelling required minimising both, but decreasing these also meant increased modelling times. If they were sufficiently small to give accurate calculations, decreasing them should have exhibited a negligible change in G_L. For the sensitivity study whether there was an increase or decrease in G_L was actually irrelevant, rather the degree of the change was of interest. The results are shown in table 4.7. Originally a time step of dt=0.025s and a cell size dz=0.001m were chosen and the G_L was calculated. The simulation for a copper baffle

with split heater in table 4.4 was again used as a basis for comparison (also shown as run 2 in table 4.6).

Table 4.7: Sensitivity Study

Variable changed	***Value***	***G_L (K/m)***	***% change over original G_L***
Original dt	0.025 s	19040.978195	/
dt / 2		19040.985589	+ 3.8×10^{-5} %
dt / 4		19041.847351	+ 4.56×10^{-3} %
dt x 2		19037.524934	- 0.018 %
dt x 4		19030.584005	- 0.055 %
Original dz	0.001 m	19040.978195	/
dz / 2		19060.185813	+ 0.10 %
dz x 2		20051.247270	+ 5.31 %

The results of the sensitivity study show that the model calculated G_L to an accurate degree. If desired the time step could actually be increased to reduce simulation time and still give accurate results, though this was not done during modelling.

4.6 - Baffle thickness correction:

In the modelling results (at least for the uncooled graphite baffle) the values for G_L may be higher than they should have been. This is because the thickness of the baffle was not considered when calculating G_L (it was included in the model but only to estimate the temperatures on the top and bottom of an uncooled baffle). When calculating G_L the model treated the baffle as a thin line, whereas to calculate the temperatures across an uncooled baffle, 5mm thickness was used as a nominal value. Therefore it could be argued the G_L values for graphite are too high as it should have been calculated over the distance between the liquidus and solidus cells *plus* the 5mm.

This relates to the temperatures on the top and bottom of the baffle, hence the same correction need not be applied to the results for the water cooled copper. In this situation the top of the baffle is shiny reflecting the majority of radiation and the water cooling holds it at a uniform, cool temperature so there will be very little or zero radiation emitted by it directly. Consequently the casting is unlikely to gain any heat via radiation from the side baffle wall (the small vertical surface concentric to the casting) or the bottom face of the baffle. As there was no temperature change across the thickness of the copper baffle, the treatment of it as a thin line in the model should be valid. Figure 4.4 illustrates how the model treated the baffles as 'thin' when calculating G_L.

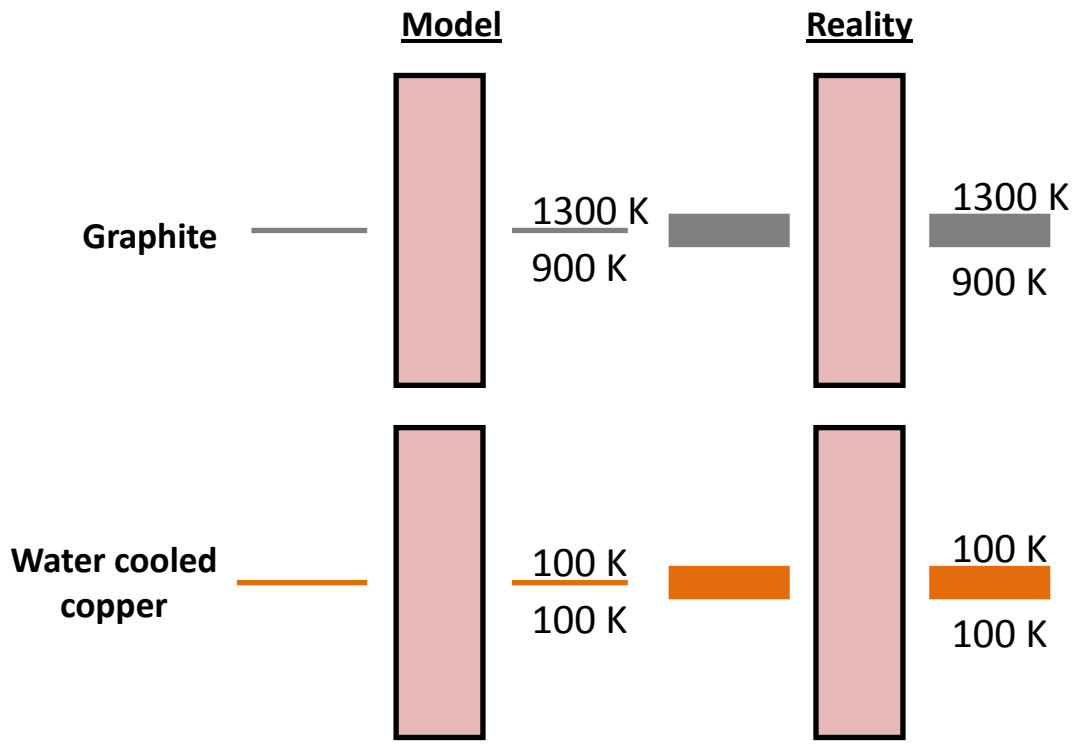

Fig. 4.4. A representation of how the model treated the baffle thickness when calculating G_L compared to reality. With no temperature gradient across a cooled baffle it does not matter the model treats it as thin, but this may affect the results for an uncooled baffle.

Applying a correction to the graphite baffle values, however, potentially means that improvements in G_L could be greater than indicated in the modelling results. The 25% potential increase in G_L from using water cooled copper as a baffle in the current setup at Birmingham, suggested by the model (when considering runs 3 and 4 in table 4.6) could be increased if a baffle correction were applied to run 3.

5.0 – PRACTICAL WORK

Since cost was an issue and the introduction of extra water cooling to the furnace was difficult, initial tests were done without it at temperatures lower than in actual casting to investigate the potential of highly reflective baffles.

5.1 – Set 1: Three part split baffle – graphite, gold & copper

The initial experiment was relatively simple and done without an actual mould in the furnace, or a withdrawal. A thermal baffle consistent with those used in a standard casting (graphite foil sheet, radius 100mm, thickness 2.16mm) was cut but with no central hole. A third of it was coated with 24 carat gold leaf, a third coated with polished copper sheet (1mm thickness) and the final third left uncoated so radiation was incident on the graphite.

The gold leaf was joined to the graphite in layers using watered down PVA glue. It was estimated that the presence of PVA would be unlikely to have any effect on radiation as it would simply turn to carbon when heated and be relatively inert (though it was unknown at the time if the gold or copper could have become unstuck at higher temperatures and if that would affect results). This technique also proved successful for joining the copper sheet to the graphite foil by clamping them together. The baffle was then cut at the interfaces between the three sections to prevent any lateral conduction (see figure 5.1).

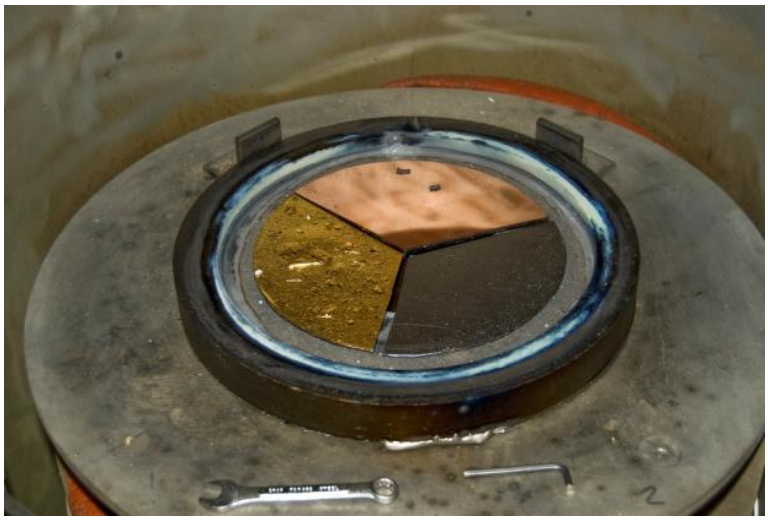

Fig. 5.1. Three part split baffle (gold leaf, copper sheet and graphite foil).

Fig. 5.2. Copper stand supporting three thermocouples under each baffle section.

Each section was positioned in the furnace independent of the others resting on a thermocouple, located on the underside. A copper stand shown in figure 5.2 was fabricated to rest on the ram and support the thermocouples. Monitoring the temperature on the underside of the sections gave an indication of how much radiation had been absorbed by each and conducted through it - lower temperatures on the gold and copper thermocouples were expected. Initially the heaters were taken to 1000^{o}C (whilst monitoring thermocouple readings) to avoid melting the copper or gold. The three thermocouple readings are shown in figure 5.3.

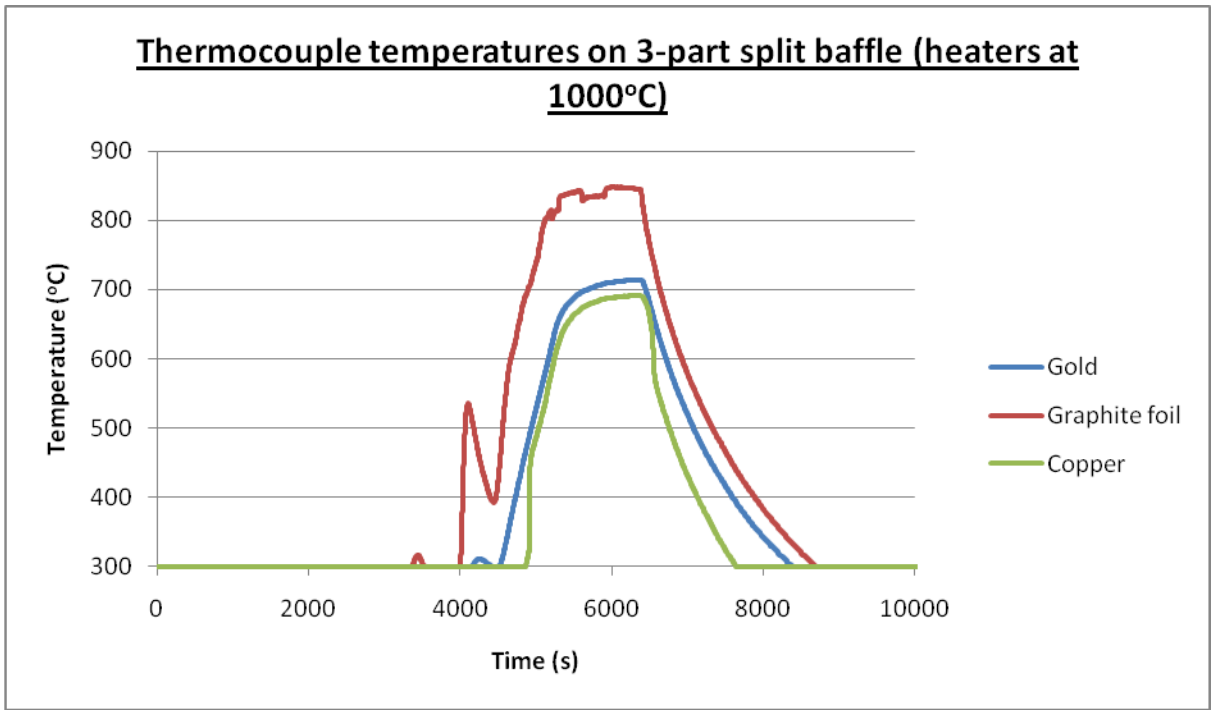

Fig. 5.3. The temperatures exhibited on the underside of the different sections of the split baffle.

5.2 – Set 2: Copper vs Graphite baffle including withdrawals

As copper exhibited the lowest temperature, it was chosen for further testing. When casting turbine blades furnace temperatures are roughly 1600^{o}C, far exceeding the melting temperature of copper. Before considering this, however, further tests were done to assess the performance of copper against graphite foil and to investigate other variables that could affect G_L. Each of these runs included a withdrawal (no actual melting and casting of an alloy was done).

The other variables changed were the clearance gap between the edge of the baffle and the mould and the size of the insulation ring that forms the base of the hot zone. These were varied independently to see if any effect on G_L was found. It was

proposed that reducing the amount of insulation may benefit G_L - the insulation has a high emissivity so it was necessary to investigate if it heated up considerably during casting, which would leave it free to emit radiation into the cold zone.

These experiments were all done using a 20mm diameter cylindrical mould (height 20cm) with thermocouples located in it and all withdrawals done at a velocity of 6.5×10^{-5} m/s. The mould and thermocouple setup can be seen in figure 5.4.

Fig. 5.4. Image showing the 20mm diameter cylindrical ceramic mould on the copper chill plate - thermocouples located in the mould to measure temperature.

The first was done using a graphite foil baffle with clearance gap 3mm (note the mould shell is not a perfect cylinder so is impossible to get a totally consistent gap) and the original insulation ring, to provide a basis for comparison. Subsequent withdrawals investigated the variables independently, keeping consistency with the first withdrawal

unless stated otherwise. In the second run the graphite foil was replaced with copper sheet (1mm thickness) with the original insulation ring and clearance gap. Similarly in the third run (copper baffle), except here the clearance gap was increased to 8mm. For the fourth run the smaller gap of 3mm was used again, but this time with a new insulation ring – this was the same as the original but with minimal inner radius (as much insulation material removed from the middle as possible), without impairing the structure of the setup. The temperature v position curves for these experiments are shown in Figure 5.5 (where the steeper the curve, the larger the gradient) and their values for G_L between 700°C and 800°C (the steepest part of the curves) are shown in table 5.1.

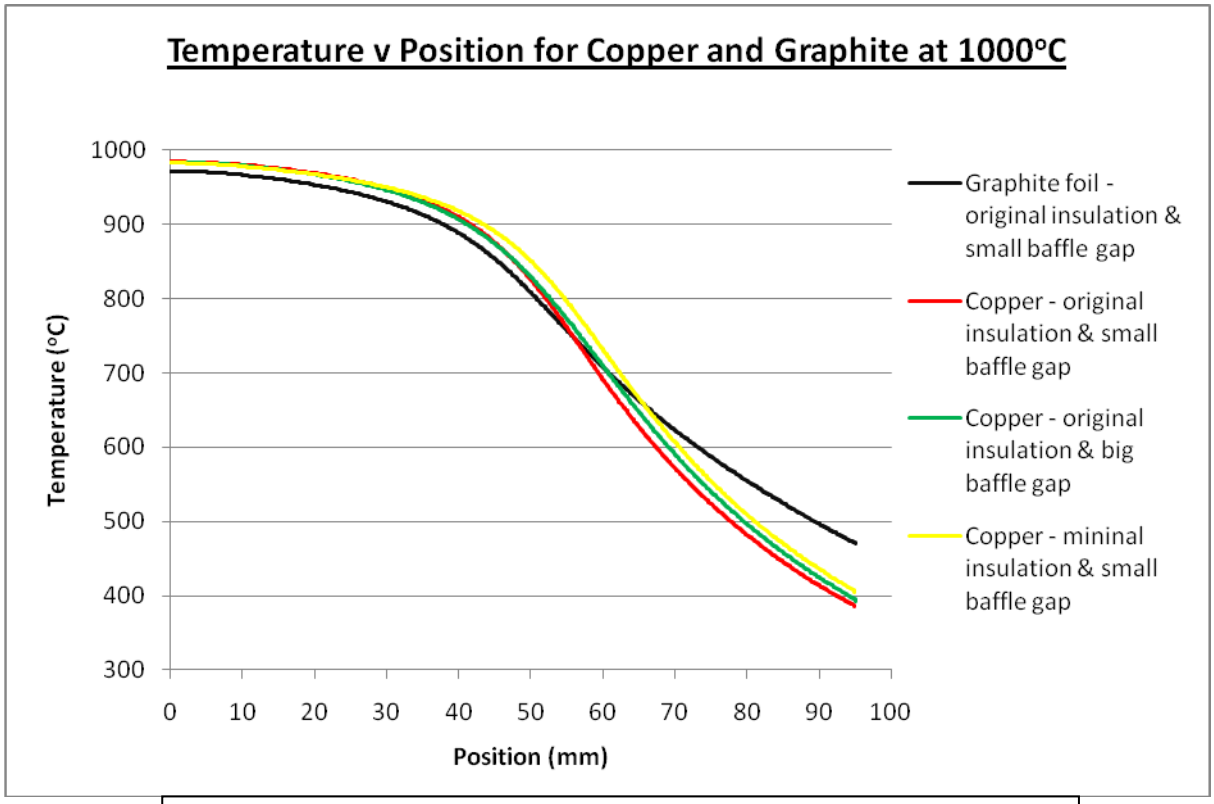

Fig. 5.5. Curves for temperature against position for the different withdrawals done. Steeper curves indicate higher G_L. Baffle material, clearance gap and insulation ring size were varied.

Table 5.1: Effect on G_L with copper baffle in the furnace at 1000°C

Withdrawal	*Variables*	*Thermal gradient (K/m) (from 700°C - 800°C)*	*% increase over graphite*
1	Graphite foil; small baffle gap; normal insulation ring.	10024	/
2	Copper; small baffle gap; normal insulation ring.	13711	+ 36.8%
3	Copper; big baffle gap; normal insulation ring.	12308	+ 22.8 %
4	Copper; small baffle gap; minimal insulation ring.	13122	+ 30.9 %

Table 5.1. Gives the values for thermal gradient calculated from the withdrawals. Solidus and liquidus temperatures of superalloys were not reached so the gradient was calculated on the steepest part of the curves from 700°C - 800°C.

5.3 – Set 3: Higher temperature operation (water cooled copper baffle)

The copper baffle exhibited improvements in G_L over the original graphite foil baffle but since the copper was near to its melting temperature with the heaters at 1000°C the next step was to investigate how to increase the operating temperature without destroying the baffle. Replacing copper with a higher melting point metal e.g. platinum (melting temperature of 1768.3°C) was one possibility, but also expensive so it was decided to continue investigation with copper. Therefore to raise the operating temperature a water cooling system was put in place to cool the baffle - this can be seen in figure 5.6 (external image of the water in and out pipes), figure 5.7 (internal furnace image of water pipes and the copper chill plate) and figure 5.8 (image showing the water pipes joined to the underside of the chill plate).

Fig. 5.6. Water pipes in and out of the Retech furnace providing water cooling for the copper baffle.

Fig. 5.7. Inside the furnace, showing the water in and out pipes and the copper chill plate used to cool the copper baffle.

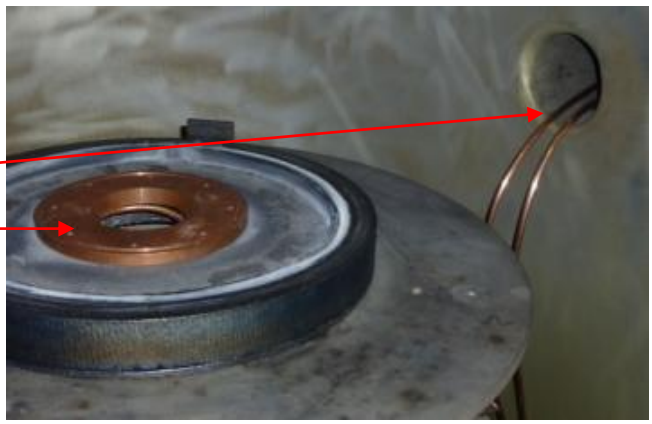

Fig. 5.8. Pipe connections made underneath the water cooled baffle. Note it was also possible to leave the insulation baffle in place.

Similarly to section 5.2, these tests were done with thermocouples in the mould however an extra two were also used for monitoring the baffle temperatures (the exact amount of cooling that could be imparted by the chill plate was unknown). These were located on the underside - one near the outer edge and the other near the inner edge of the baffle.

The copper chill plate (figure 5.7) was central but of smaller diameter than the baffle, meaning the baffle's outer edge needed to be monitored most carefully.

To situate these thermocouples, holes were made in the insulation ring and the thermocouples threaded through. They were secured in place so the baffle was resting on them. The baffle was then screwed in place to give the best possible contact between the copper and thermocouples (as well as optimal conduction to the chill plate) as can be seen in figure 5.9.

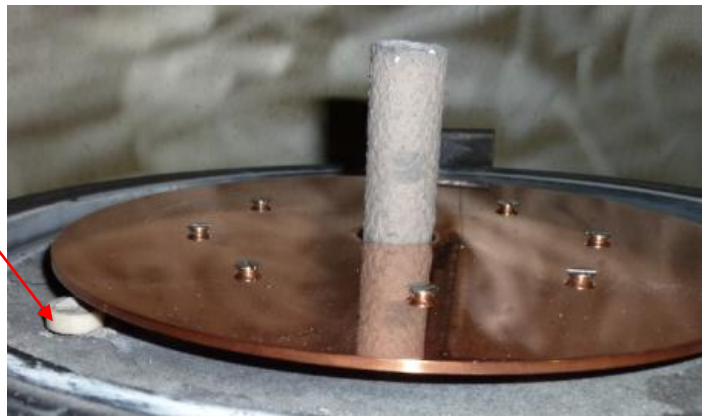

Fig. 5.9. Thermocouples located under the water cooled baffle; baffle screwed down to chill plate for good contact.

These tests aimed to use a highly reflective copper baffle (figure 5.10) at furnace temperatures exceeding its melting point and record a withdrawal without destroying it. A thicker copper sheet (3mm) was used to benefit conduction to the chill plate. Water pipes in and out of the furnace were added and the baffle located on top of the copper chill plate. As there was some uncertainty in exactly how much cooling the chill plate could impart, the temperature in the furnace was increased gradually and the thermocouple data was carefully monitored throughout the experiments.

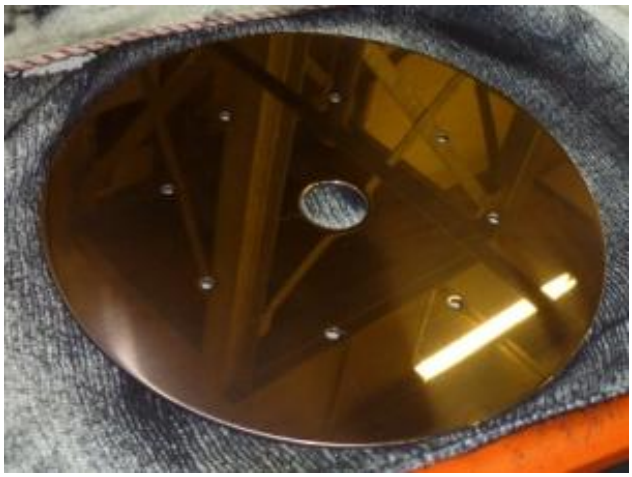

Fig. 5.10. Highly polished reflective copper baffle for use with the water cooled chill plate.

5.3.1 - Water cooled baffle – 1000°C:

The furnace was set up and the heater raised to 1000°C to ensure the new baffle set up survived at that temperature. The baffle survived without any problems but as can be seen from figure 5.11, the temperature on the outer baffle thermocouple rose to around 850°C.

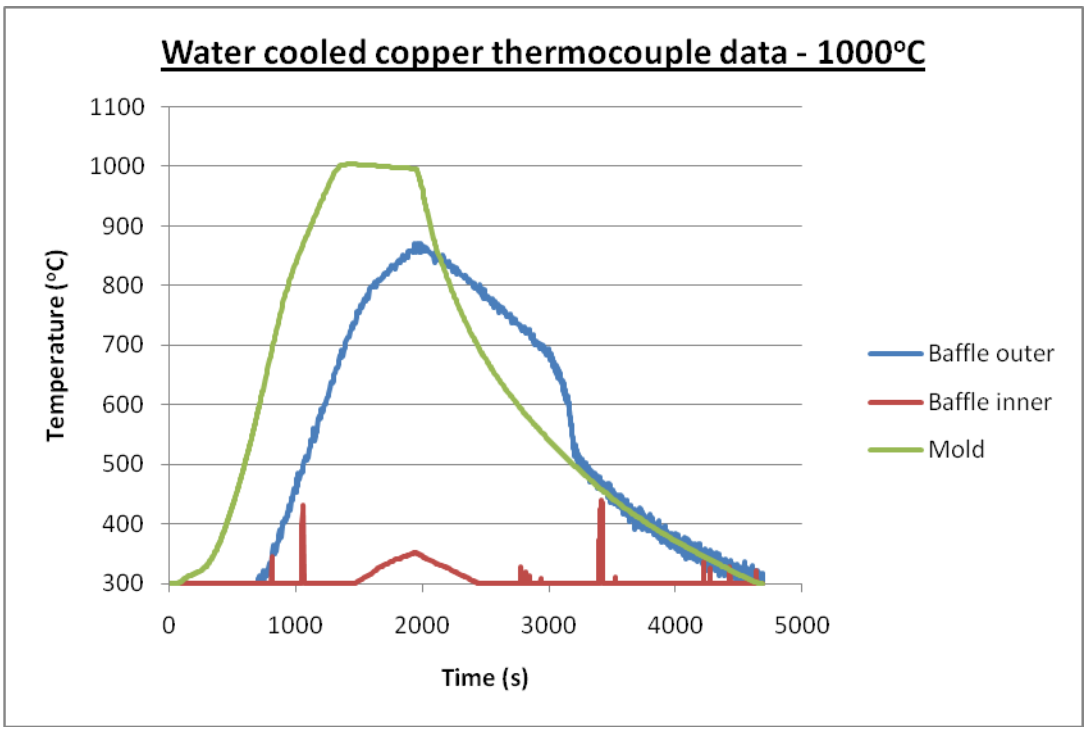

Fig.5.11. Thermocouple data when water cooled copper baffle was taken to heater temperatures of 1000°C.

5.3.2 - Water cooled baffle – 1300°C:

Next the heater temperatures were raised to 1300°C. This run had to be cut short however - during heating the temperatures on the baffle outer thermocouple suddenly shot up very high (see figure 5.12), so the heaters were turned off and the furnace opened up. It was found that the baffle had touched the heating element and started to melt but only on one side. This baffle is shown in figure 5.13.

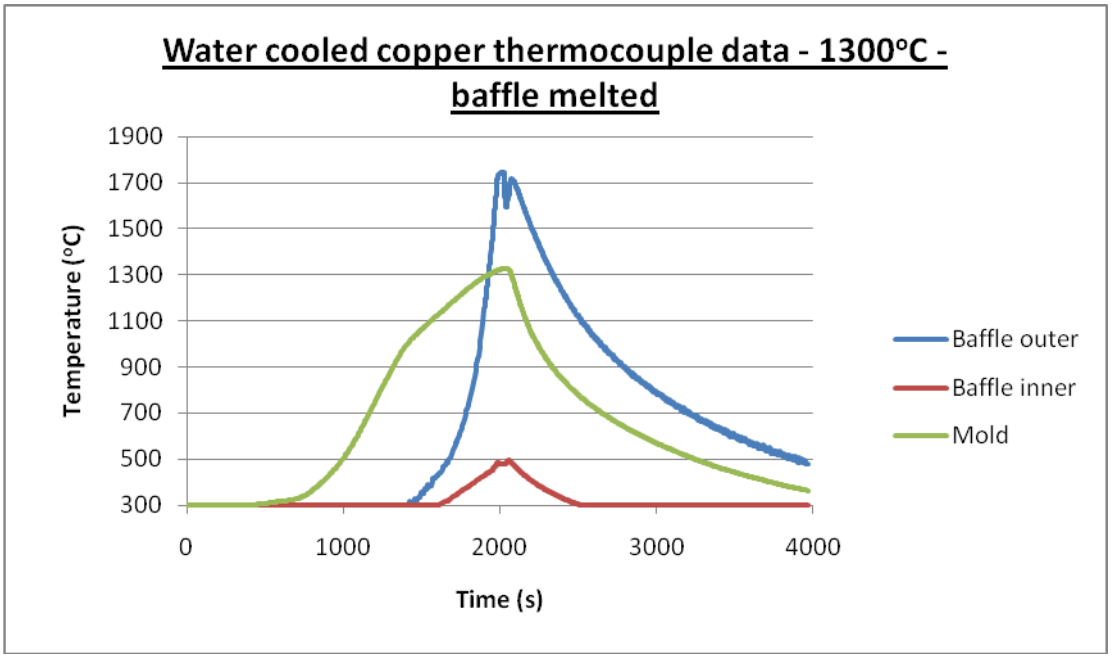

Fig.5.12. Thermocouple data when water cooled copper baffle taken to heater temperature of 1300°C. The edge started to melt - note baffle outer temperature increases to almost 1800°C – the heaters were not even this high so the melted copper may have damaged the outer baffle thermocouple.

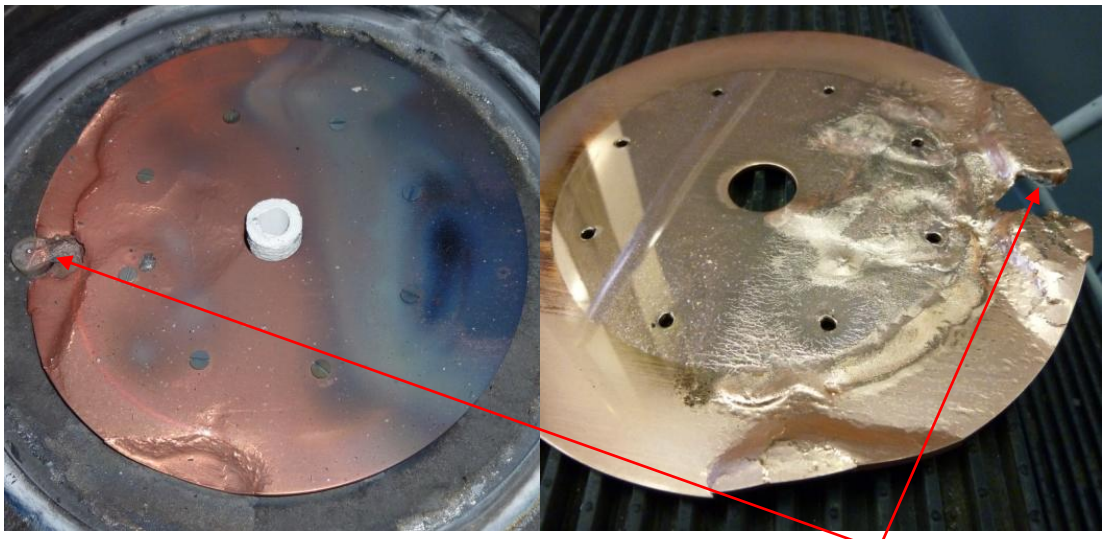

Fig. 5.13. The first thicker copper baffle that was partially melted at the edge as it was in contact with the heating element - perhaps the thermocouple underneath the baffle pushed the edge of the baffle up.

5.3.3 - New water cooled baffle – 1300°C:

The melted baffle was replaced (two similar baffles had been prepared in-case of such a situation) but this time a couple of millimetres of the insulation ring below the baffle (highlighted by the arrow in figure 5.14) was removed (allowing the baffle to be lowered hence give more clearance between itself and the bottom of the heater). The heaters were then raised to 1300°C (no withdrawal done) to make sure the baffle did not melt this time, which proved successful.

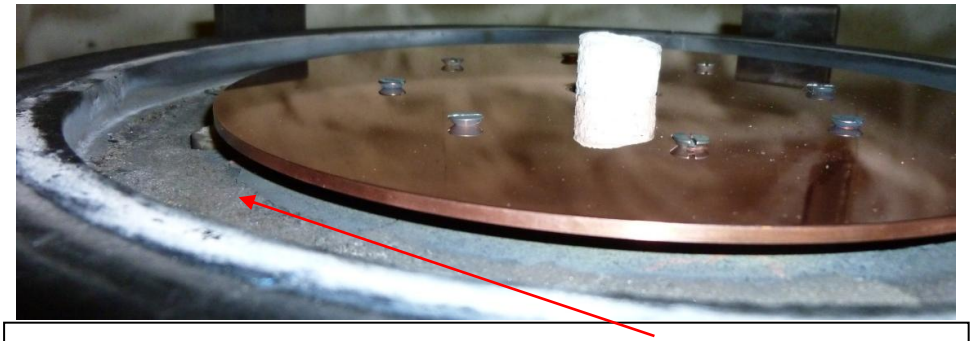

Fig. 5.14. Shows the baffle sat above the insulation ring - some of this material was removed to accommodate the baffle and chill plate.

5.3.4 - Water cooled baffle – 1300°C, withdrawal done:

After establishing the chill plate provided enough cooling to go to 1300°C operating temperature, this was repeated in the fourth run but a withdrawal was done hence a thermal gradient could be plotted (see figure 5.15). The gradient found between 800°C - 1000°C was 18721 K/m. The baffle temperatures were recorded for this run but they were found to be unreliable so are not included.

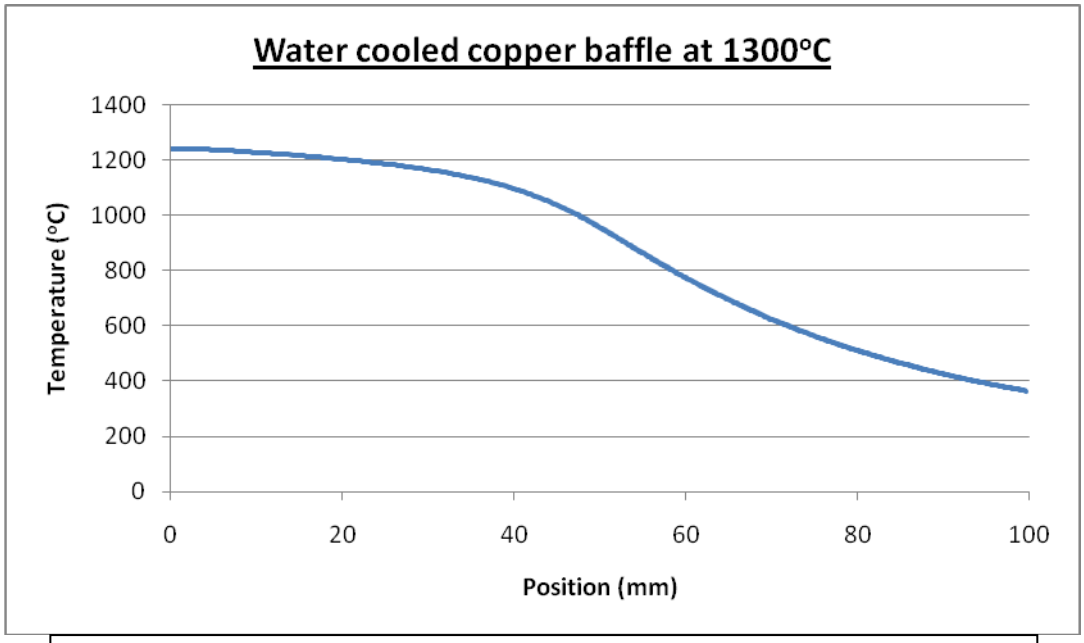

Fig. 5.15. The temperatures recorded on the mould thermocouple during the withdrawal at 1300°C heater temperature using the 3mm thick water cooled copper baffle.

6.0 - DISCUSSION:

6.1 – Set 1: Three part split baffle – graphite, gold & copper

The thermocouples under the gold and copper sections gave readings considerably lower than that on the graphite foil section, indicating both materials have potential for reducing the heat emitted by the baffle into the cold zone and retaining more in the hot zone.

Copper exhibited the lowest temperature of all despite it being expected gold would perform better (emissivity of gold is nominally slightly lower). This may have been due to the fact that layered gold leaf was used as opposed to sheet material for the copper. Emissivity is dependent on material and surface finish and whilst the layered gold leaf was still shiny in appearance, there was less potential for it to be polished and smoothed as finely as gold sheet would. Also upon removing the baffle after heating, it was found that the layers of gold leaf had started to flake off under the elevated temperatures affecting the surface, which may have had some impact on results. This can be seen in figure 6.1.

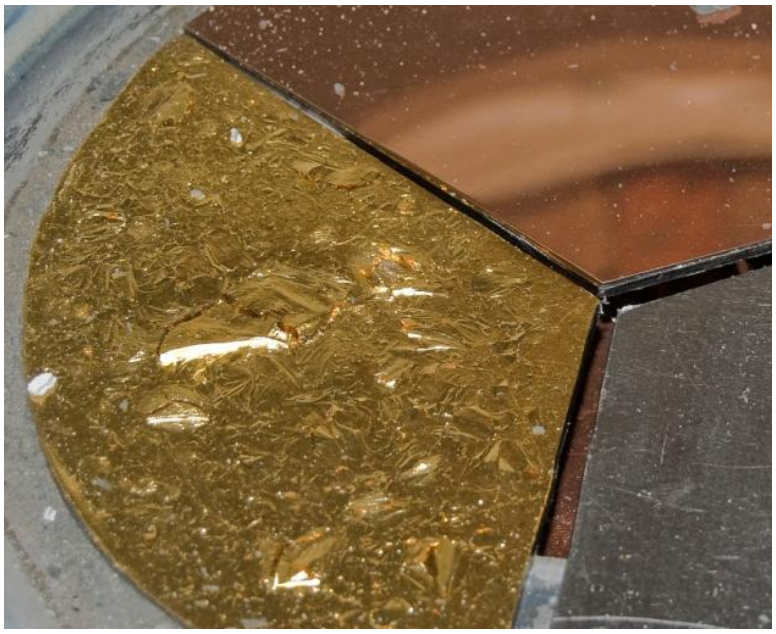

Fig. 6.1. Gold leaf exhibiting flaky surface finish after heating in the furnace.

Despite this, due to the fact that the copper did perform better in the initial test and that gold has only a slightly higher melting point, a slightly lower emissivity (potentially) and is more expensive, it was decided that the possible benefits (if any) of even a very highly polished gold sheet over copper would be minimal and for the purpose of testing the theory it would not be cost effective to use gold. Therefore copper was selected as the material for further investigation.

6.2 - Set 2: Copper vs Graphite baffle including withdrawals

As can be seen from the steeper curves in figure 5.5 the copper baffle gave steeper gradients than the graphite foil when a withdrawal was done at 1000^{o}C (heater temperature). This was consistent in all the withdrawals done with copper. Initially the graphite curve follows a similar kind of shape to the others, but below around 750^{o}C the thermocouple appeared to cool at a slower rate. This is perhaps indicative of the

reflective copper working as predicted and being a more effective thermal barrier. From withdrawal 1 to 2 the central hole in the graphite foil and insulation used were the same size so it is proposed that the slower cooling rate with a graphite baffle is due to the baffle absorbing radiation, conducting the thermal energy through it then emitting from its base into the cold zone, where it could be incident on the mould and hinder cooling. The thermal gradient measured between 700-800^{o}C suggested an improvement of 36.8% from using copper over graphite alone. Furthermore, the maximum temperature on the mould was slightly higher in all three copper withdrawals than the graphite one, suggesting the highly reflective surface also aided the heating of the mould while it was in the hot zone. Note that all withdrawals were done with a hollow ceramic mould so values for G_L were higher than would be expected in an actual casting with HRS as there was no vertical conduction in the superalloy, which would reduce the gradient.

In terms of the varied baffle gap and size of the insulation ring, there was only a slight difference exhibited between the three copper withdrawals. The copper baffle with the bigger clearance gap (withdrawal 3) had a gradient around 10% lower than withdrawal 2. This had less effect than changing the baffle material but the clearance gap is still an important parameter to be minimised. The mould used was a 20mm cylinder of constant cross section, unlike actual turbine blades where the gap will vary during withdrawal. It was decided not to investigate this further but to simply keep the baffle gap at a minimum for subsequent tests as this topic has been covered in the literature (Liu et al., 2010).

The results suggest reducing the insulation material below the baffle did not give any benefit to G_L (around 4.5% lower in withdrawal 4 than withdrawal 2), indicating it probably acts to prevent heat conducting into the cold zone (as it is supposed to) rather than heating up and emitting from its surfaces. However the difference in G_L was very small so to give an accurate conclusion on this further detailed testing with thermocouples in the insulation would be ideal - this was decided not to be worthwhile however.

6.3 – Set 3: Higher temperature operation (water cooled copper baffle)

After melting the first baffle (problem was easily solved by removing a small amount of the insulation ring below), the next baffle survived at 1300^{o}C (heater temperature), so a withdrawal was recorded at that temperature.

Analysis of the thermocouple data from the final two runs in this set (section 5.3.3 and 5.3.4) however showed that the baffle temperatures recorded (at least from the outer baffle thermocouple) were unreliable. This can perhaps be attributed to the fact that in the second run the copper melted localised to the region of the thermocouple. This perhaps damaged it and caused it to give incorrect readings for the two subsequent runs, as a withdrawal was completed without damaging the baffle but the thermocouple suggested the temperature had risen above copper's melting point, as can be seen in figure 6.2.

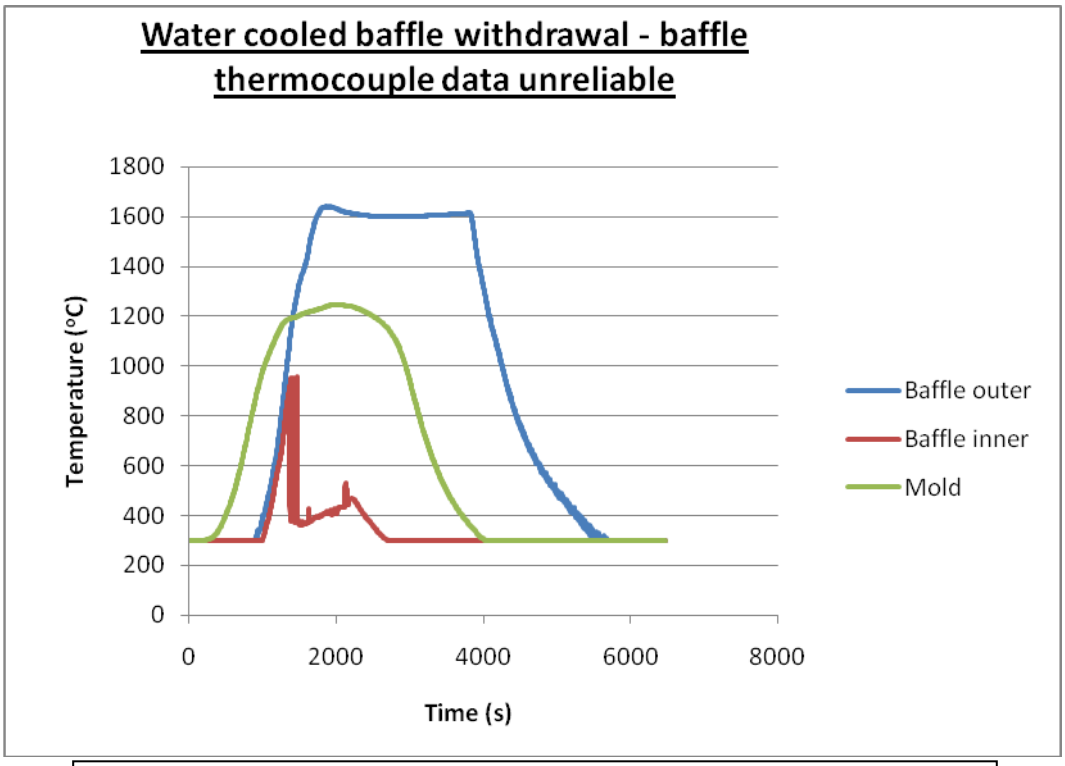

Fig. 6.2. Shows the unreliable thermocouple data when withdrawal was done at 1300°C. The copper did not melt so clearly at least the outer baffle thermocouple gave incorrect readings.

Since at 1000°C the thermocouples showed temperatures of around 850°C on the baffle and in the final withdrawal the inner baffle temperature approached copper's melting point (though whether this thermocouple was also damaged is unknown), it was decided not to attempt raising the operating temperature further with the current set up. To use copper at a normal casting temperature of 1600°C, an improved water cooling system was required (the copper chill plate used at 1300°C had a much smaller outer radius than the baffle, so only the inner part of the copper baffle was cooled effectively by it).

Ideally a similar withdrawal using a graphite baffle would have been recorded to compare the increase in gradient at 1300°C with that at 1000°C. This was not possible however due to inavailability of the furnace, but the tests done at 1000°C show there is

potential for improved G_L with the use of reflective baffles and this run shows copper baffles can survive at heater temperatures above their melting point. Raising the operating temperature to a realistic casting temperature of 1600^{o}C was the main obstacle to the use of the copper baffle and testing the behaviour at this temperature would have been much more informative had the baffle chill plate provided enough cooling.

In DS the temperature gradient across the solidification range is really of interest. The crystallisation of Ni-superalloys, however, occurs above the temperatures the furnace has so far been raised to. Nevertheless a value for G_L of 18271 K/m (between 800-1000^{o}C) at a heater temperature of 1300^{o}C for the water cooled copper baffle was found.

Fig 6.3. Deposits found on the copper baffle after withdrawal at 1300^{o}C.

An interesting finding was that the reflective surface of the shiny baffle was dull after the withdrawal at 1300^{o}C due to deposits on it – in parts it was even black as can be seen in figure 6.3 (at the previous runs to 1000^{o}C without water cooling no deposits were found on the copper). This is obviously an issue for the re-usability of such components

(although the structural integrity of it was not impaired) but the re-polishing of baffles after every single use may or may not be worthwhile, depending on how much improvement in G_L they can offer at actual casting temperature. Also if the deposits occurred during the casting process then the emissivity and amount of radiation reflected by the surface of the baffle may actually have been reduced as more of the casting withdrew and the deposits increased. Potential sources were perhaps the graphite resistant heating element or the presence of the screws or some part of the water cooling system (as no deposits were found at 1000^{o}C without these).

6.4 - Higher melting point metals

Platinum has been mentioned as an ideal but expensive candidate for low emissivity baffles and at temperatures of 1600^{o}C would not even require the use of water cooling (melting point of 1768°C). Had a significantly improved G_L been found at 1300^{o}C with a copper baffle over graphite, this may have justified the cost of investigating platinum baffles, or even a platinum coating for a water cooled copper baffle. This potentially would allow testing at 1600^{o}C and analysis of the microstructural benefits with an actual superalloy casting.

7.0 – COMPARISON OF MODEL WITH PRACTICAL

Simulations were done using the model to represent the practical runs done in the furnace. The runs at 1000^{o}C were focused on to give a comparison of a withdrawal with both graphite and copper baffle materials. In the furnace tests the thermocouples were located in a hollow mould so the casting properties were changed to simulate this (metal was included in the previous modelling) and the properties in table 7.1 were used.

Table 7.1. Mould properties:

ρ (kg/m3)	*C_p (J/kg/K)*	*ε*	*K (W/m/K)*
2750	1000	0.7	2.5

(Elliot and Pollock, 2007)

Other variables:

The following variables were changed from the previous modelling runs. Unless stated here all other variables are consistent with those described in section 4.3:

- Values of solidus and liquidus (used in the model for calculating G_L) changed to 700^{o}C and 800^{o}C respectively to calculate GL over the same range as done in table 5.1.
- Heater temperature set to 1000^{o}C.
- Top of furnace set to 900^{o}C.
- Mould emissivity 0.7 used – no superalloy in furnace withdrawals so no correction in the model for mould emissivity (see figure 7.1).

Fig. 7.1. Since the mould is a hollow tube, not a solid bar this had to be accounted for when considering the conduction. The tube was 10mm outer radius, 6mm inner radius, so thickness of ceramic tube was 4mm.

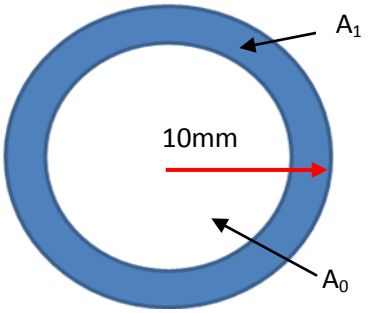

The conductivity would be given by:

$$A_{TOTAL}k_{TOTAL} = A_0k_0 + A_1k_1$$

Presence of vaccum means k_0=0, therefore:

$$\pi 0.01^2\, k_T = \pi 0.006^2\, k_0 + \pi(0.01^2 - 0.006^2)k_1$$

With a 4mm thick wall, k_T = 0.6 k_1 so if k_1 = 2.5 (Elliot and Pollock, 2007), this gives a corrected mould emissivity of: $k_T = 0.6 \times 2.5 = 1.5$

These values were then used to model a withdrawal of a hollow ceramic mould at 1000^{o}C with firstly a 2.16mm thick graphite baffle, then a 1mm thick reflective copper baffle. G_L was calculated from each set of results between 700^{o}C and 800^{o}C and compared with the experimental results (see table 7.2) – this range was chosen as this is the steepest part of the curves, shown in figures 7.2 and 7.3 for graphite and copper baffles respectively.

Table 7.2. Model v Practical:

	Thermal gradient (K/m) between 700°C and 800°C	
	Furnace results	***Modelling results***
Graphite (2.16mm thick)	9987	12529
Copper (1mm thick)	13617	23624
Improvement in G_L over graphite	36%	88%

Table 7.2. Note that all of the values are higher than what has been found in the literature with the HRS process. This is to be expected as there is no superalloy charge present, which would increase the vertical conduction and act to lower G_L.

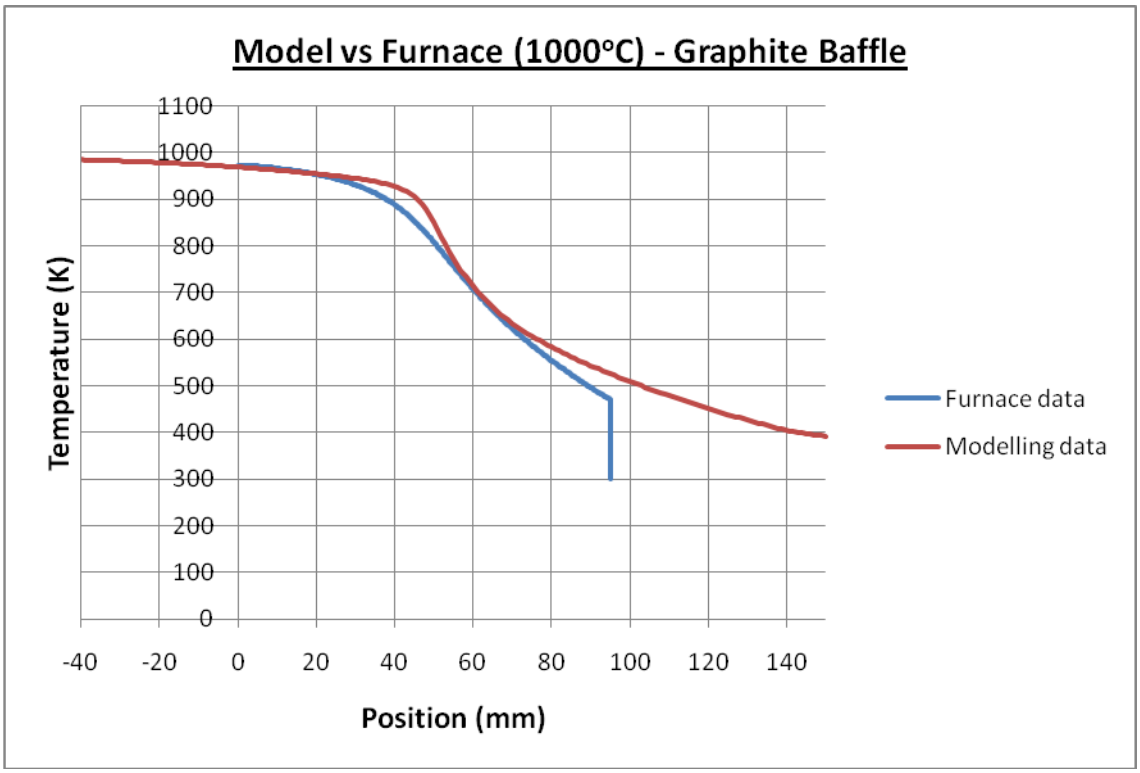

Fig.7.2. Temperature vs. position for the data obtained from the modelling and practical tests for traditional graphite baffle material. The curves are quite similar, particularly in the region of the baffle. Note the thermocouples used in the furnace did not take readings below 300°C so that is why the furnace data temperature data stops there.

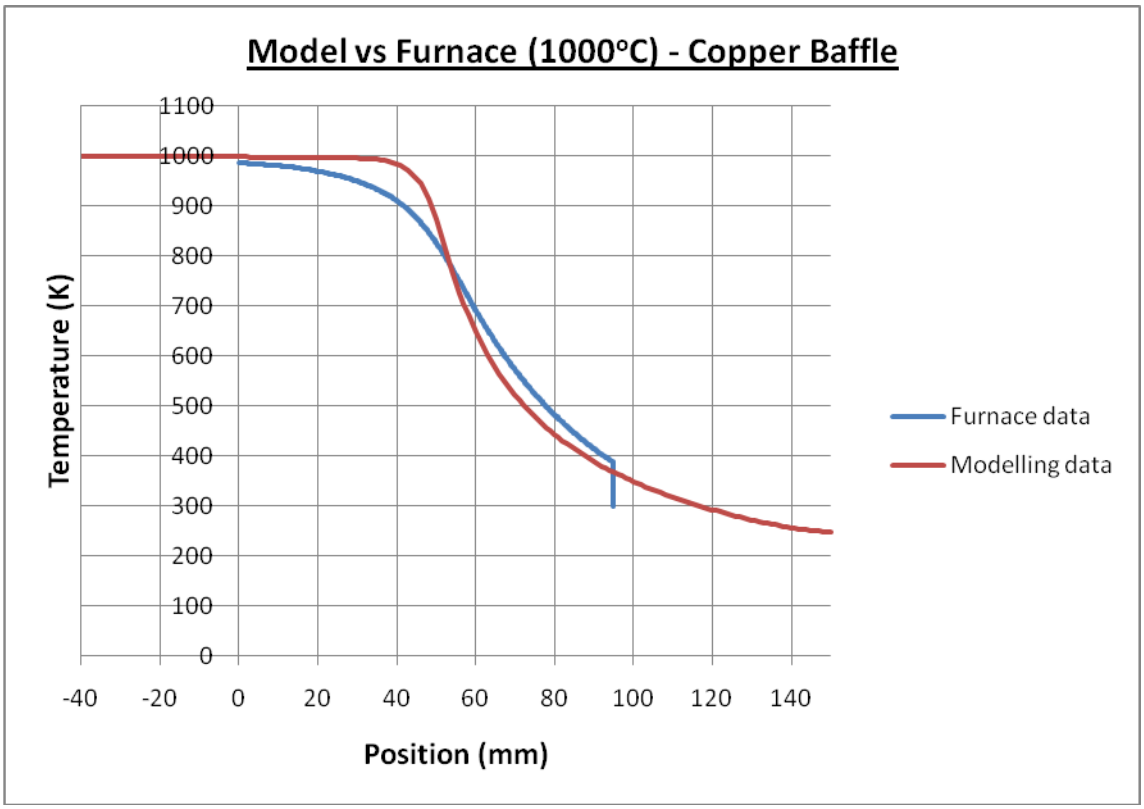

Fig.7.3. Temperature vs. position for the data obtained from the modelling and practical tests for reflective copper baffle material. The curves are quite similar, but do not match as well as the curves for graphite.

7.1 - Discussion:

The values for G_L calculated by the model were higher than the values found experimentally, indicating the model was not entirely accurate, although it can be seen from the curves that the gradient found by the model was reasonably accurate.

7.1.1 - Baffle thickness correction:

As discussed in section 4.6 it may be reasonable to assume the model values for G_L were slightly higher than they should be due to the model not taking the baffle thickness into account when calculating the gradient. Since both withdrawals done at 1000°C (graphite and copper) were with uncooled baffles this could also apply to these modelling

simulations of the practical runs. This may account for the higher G_L values from the model.

The experimental data found at 1000^{o}C suggests an improvement of around 36% in G_L using copper (and this was not even water cooled so potentially may have emitted some heat into the cold zone). By correcting the model's result for the graphite baffle, however, the improvement suggested by the model may be closer to the improvement found in the practical testing. Ideally a test at 1600^{o}C would be used to compare the improvement in G_L with that suggested by the model. The model does show the correct trends so for these reasons the correction has not actually been calculated although it is important to be aware this may be a factor affecting the modelling results.

7.1.2 – Thermocouples – inside vs. outside mould surface:

The model was more accurate when calculating the gradient for a graphite baffle than copper - for both types however in the region of the baffle at least the results from the modelling are very similar to the practical. For copper the curve from the model in figure 7.2 suggests increased overheating above the baffle as well as slightly more rapid cooling - possibly to do with how the model takes into account the reflectivity of the baffle.

This may possibly be explained by the location of the thermocouples in the mould in the practical tests. In reality, the presence of the metal in the thermocouple wires would act to increase the conduction along the vertical axis of the casting (even if only slightly) and reduce G_L. When modelling this was not included so may account for the higher gradients found. There was a smaller difference with the graphite baffle but the

gradients were generally lower - with a larger gradient the conduction effect along the wires would be more profound hence a greater difference in the gradient with the copper baffle might be expected.

In reality, the mould is not all at the same temperature. The model was concerned with the temperature of the outside of the mould but the thermocouples in the practical were located inside, measuring the inner wall. Due to conduction through the thickness of the mould it may be true that the gradient on the inside wall is lower than the gradient on the outside, which could also possibly explain the higher values.

7.1.3 – Thermocouple position in relation to baffle:

Another point to consider is the position of the thermocouple in relation to the baffle. In the practical it started off above the baffle with a certain distance X (m) of the casting above the baffle. As withdrawal occurred the casting and thermocouple moved down with X decreasing until the mould was entirely in the cold zone. In the model results presented however the mould was kept with 10cm above and below the baffle at all times, and the temperature gradient along its length was reported, which may have affected how the model compares to reality.

7.1.4 – Thermocouple readings vs. actual heater temperatures in furnace:

Another piece of current work has shown that the bottom of the heater in the furnace at Birmingham does not get as hot as the control thermocouples read (Green, Personal communication 2011). This means the temperature values from the furnace data were in

reality at a slightly lower heater temperature than recorded by the thermocouples, which may have lowered G_L. For an entirely accurate comparison with the model the Retech furnace heater temperatures should have been slightly higher than those input to the model to simulate this, which may have made the results match better.

To check how this might have affected the comparison, the two furnace withdrawals were simulated again, only this time a correction for the heaters was made in the model, with the heater temperatures reduced by 50^{o}C (single part heater was used), for both the graphite and copper baffles. The corrected curves can be seen in figures 7.4 and 7.5 for graphite and copper respectively.

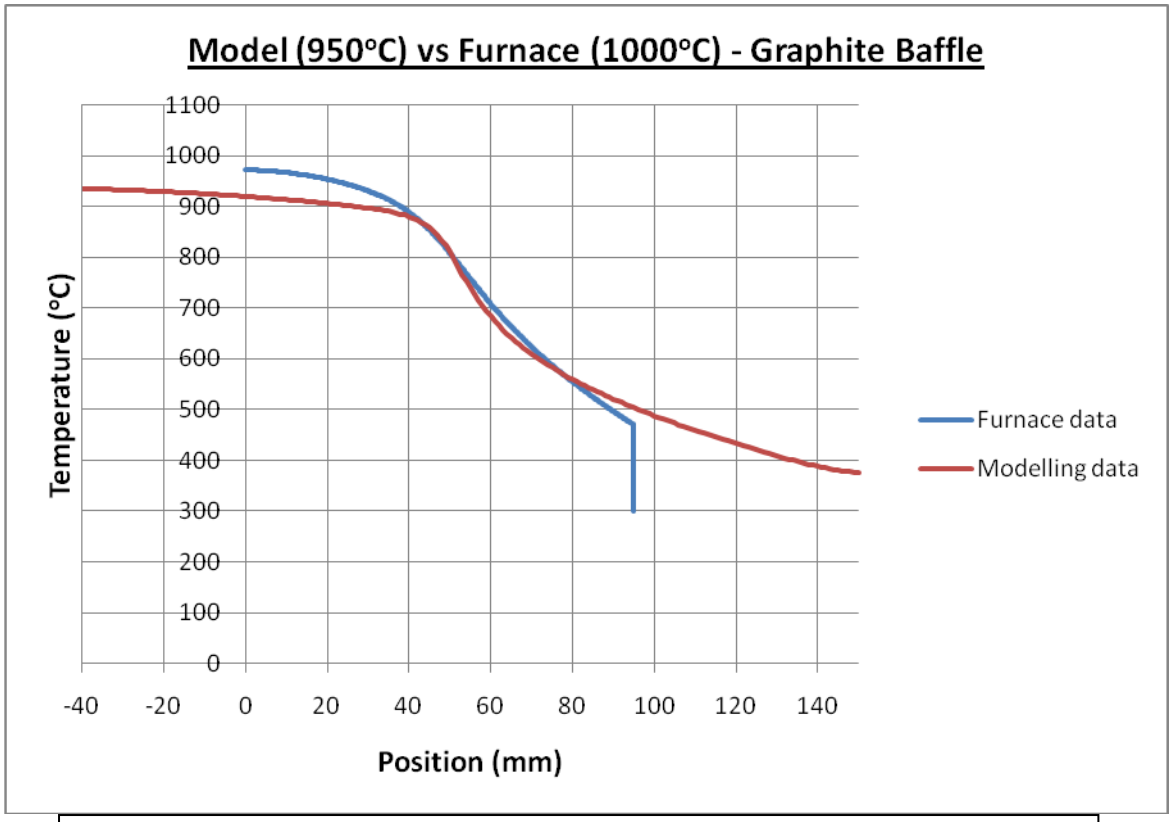

Fig.7.4. Temperature vs. position for the modelling and practical tests for graphite baffle material, with corrected temperatures in the modelling simulation. The curves are very similar.

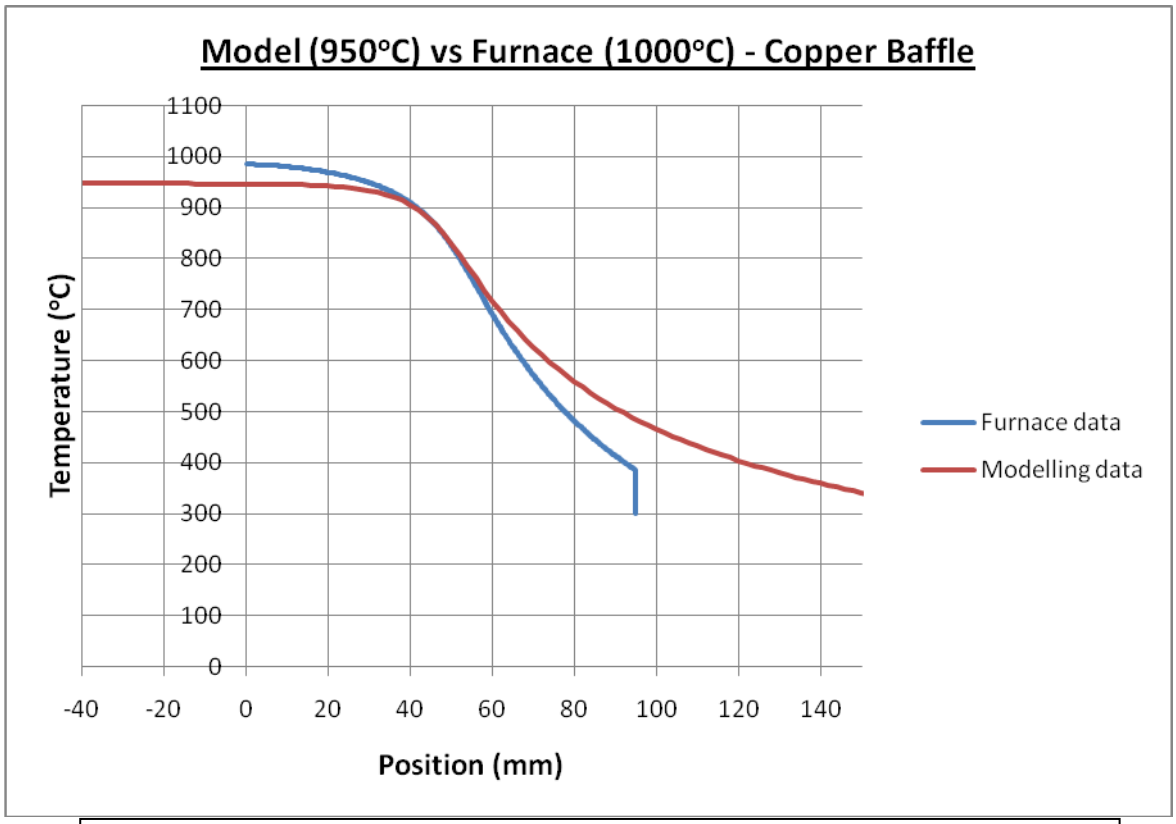

Fig.7.5. Temperature vs. position for the modelling and practical tests for water cooled copper baffle material, with corrected temperatures in the modelling simulation. There is still a slightly larger difference than in the graphite results but even so the curves are very similar.

Clearly from figures 7.4 and 7.5 with the corrected heater values in the model, the data matches the practical data better. There is still some difference, and the graphite baffle results match better over the range of temperatures – the copper in the model still appears to cool slower than in reality however the data for both materials matches closely in the region of the baffle, which is the main area of interest as the mushy zone is expected to be near the vicinity of the baffle.

7.2 - Primary dendrite arm spacing λ(m):

λ is proportional to the solidification range and $G_L^{-1/2}v^{-1/4}$ (Reed, 2006, p.146), meaning raising G_L decreases λ. The increase in gradient from the results can then be used to predict the decrease in dendrite arm spacing that would result, as follows:

$$\lambda \propto G_L^{-1/2}v^{-1/4} \qquad [5]$$

For a given alloy and constant velocity any changes the effect of raising the gradient on λ can be shown by:

$$\lambda = C_1.G_L^{-1/2} \qquad [6]$$

Where the term C_1 is a constant dependent on the specific alloy and velocity used. The arm spacing will decrease by factor x if G_L increases by factor y as follows:

$$x.\lambda = C_1(y.G_L)^{-1/2} \qquad [7]$$

Using [7], analysis of the predicted improvements in dendrite arm spacing from the modelling and practical results is shown in table 7.2

Table 7.3. Improvements in G_L:

Run	***Heater type***	***Baffle material***	***Tgrad K/m***	***% increase in G_L over graphite***	***v m/s***
Modelling optimiser results (Table 4.6)					
1	Split heater	Graphite	15370.67	/	6.5e-5
2		Copper	19040.98	+ 24 %	6.5e-5
3	Single heater	Graphite	14597.18	/	6.5e-5
4		Copper	18218.12	+ 25 %	6.5e-5
Practical results at 1000^oC (Table 5.1):					
1	Single heater	Graphite	10024	/	6.5e-5
2		Copper	13711	+ 37%	6.5e-5

Therefore with a 25% increase in G_L (from model results), the new λ will be given by:

$x.\lambda = C_1(1.25G_L)^{-1/2}$

x = 0.89, suggesting a possible decrease of around 11% in λ.

With an increase of 37% (from furnace results at 1000^{o}C), the new λ will be given by:

$x.\lambda = C_1(1.37G_L)^{-1/2}$

x = 0.85, suggesting a possible decrease of around 15% in λ.

Again there was a slight difference found between the modelling and practical results – the reasons discussed in section 7.1 account for this - but they suggest reasonably similar values for the potential decrease in λ. A 15% decrease in dendrite arm spacing is less than hoped would be found, however it is still a considerable improvement from the use of reflective baffles.

In the literature (Reed, 2006, p.126) found that castings produced with a HRS process exhibited primary dendrite arm spacing of 100-500µm and (Liu, 2010) showed that at elevated thermal gradients and cooling rates with the LMC process, a considerable decrease in λ was found with primary dendrite arm spacing in the range 37-50µm. Applying the predicted decrease (15%) in λ from using the reflective water cooled baffle, this would give dendrite arm spacing in the range 85-425µm for HRS and 31-43µm for the LMC process.

8.0 - CONCLUSIONS:

An effective model has been produced to indicate the trends on G_L during DS casting. The focus was on varying the baffle material and temperature although it is versatile enough to investigate all variables. There is room for improvement as there are slight differences between the modelling and practical results, but the model calculates very accurately the radiation and has the ability to simulate reflective materials in the DS furnace, which is difficult with ProCast.

The theory that low emissivity, reflective baffles can improve G_L over traditional graphite foil material has been shown to be true in the Retech single shot furnace using a copper baffle at 1000^{o}C, with the results suggesting increases of G_L up to 37% possible, leading to a predicted decrease in primary dendrite arm spacing of up to 15%. Testing done at 1300^{o}C has also proved such baffles can be effective above their melting temperature if sufficient water cooling is present.

A design has been proposed for a copper baffle with improved water cooling to operate at turbine blade casting temperatures of around 1600^{o}C. Further investigation is required to see the actual improvements in G_L that could be achieved at such temperatures to indicate if this could be commercially viable.

9.0 – FURTHER WORK

9.1 - Higher temperature copper baffle:

To raise the operating temperature further to 1600^{o}C, improved water cooling would be needed as the chill plate only came into contact with the central part of the copper baffle. To achieve this, a new baffle design has been proposed where the water cooling channel is incorporated into the baffle itself to maximise the cooling area and ensure uniform cooling. Water pipes in and out would be fitted directly to the underside of the baffle. This was also designed as a split baffle that would allow it to be removed from the furnace independently of the mould (as required in actual blade casting).

The design has been developed with Solidedge CAD software and can be seen in figure 8.1, which shows one half of the split baffle. The water path was designed so that maximum cooling of the component is inferred. The baffle was also designed as thick as possible to fit within the confines of the furnace, with the idea that the thicker baffle would allow a larger surface area in contact with the water and maximise the cooling effect. Note that in the literature it has been found that thicker baffles act to reduce G_L but with a water cooled baffle, for the reasons discussed in section 4.6, this may not be the case. Even if the thickness of the design proves to be detrimental it could subsequently be reduced. The idea proposed has the water channel milled out with a lid exactly the same shape as the channel to be electron-beam welded. Water in and out pipes would be welded to the lid and holes drilled through to allow the flow of water. In the furnace the baffle would be upside-down to the image shown, so the lid and water

pipes would be on the bottom allowing the flat face on top to be highly polished and reflective.

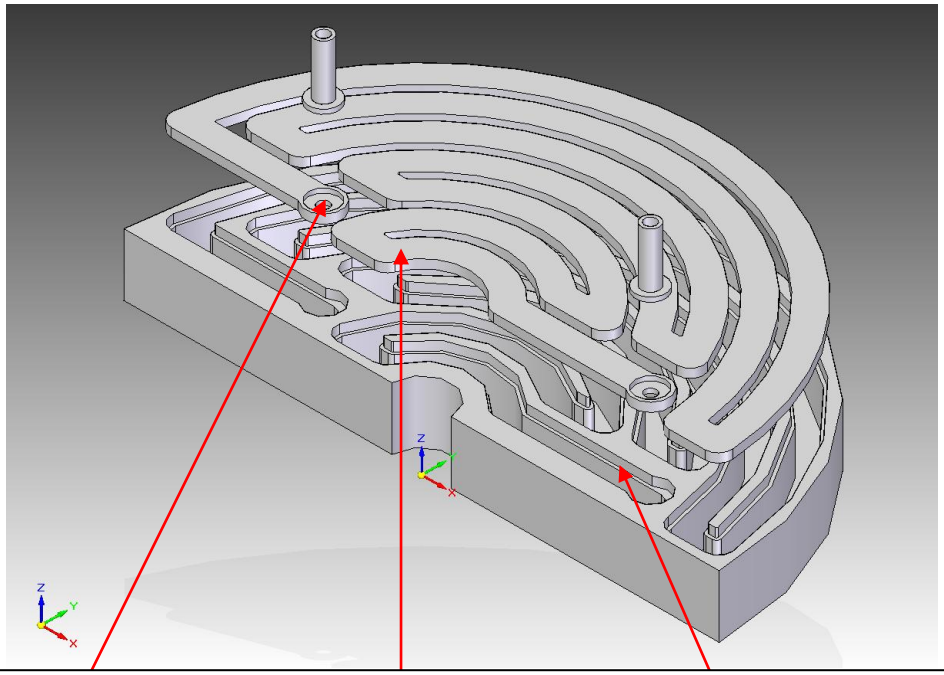

Fig 8.1. Proposed baffle design for a high temperature water cooled copper baffle. Key features are the complex shape of the water channel and lid, the holes drilled for water in and out pipes and the lip for welding the lid to the base of the baffle.

Producing and testing this part in the Retech furnace at 1600^{o}C would have been an ideal conclusion to the work to indicate whether this could be commercially viable. Had a reasonably improved G_L been observed it would have justified an actual casting and analysis of the scale of the microstructure to verify that the higher gradient imparted by the baffle led to better structural characteristics. Nevertheless improvements were seen in G_L in the lower temperature runs, suggesting that the idea has potential and is worth further investigation. Exactly how much improvement at an actual casting temperature remains to be seen but the proposed baffle design is expected to have sufficient cooling to withstand these higher temperatures without melting the copper.

9.2 - Deposits on the copper baffle

A successful run of the design at 1600^{o}C would also have justified work investigating the re-usability of such components i.e. identifying the composition and source of the deposits found on the surface of the copper baffle (figure 6.3) and whether they could be prevented or if such components would need re-polishing after every use.

9.3 - Development of the model

The model showed the correct trends but there is room for improvement, since the values for G_L were all higher than expected. Although certain approximations can be used to make the results more realistic (e.g. for the emissivity values), developing the model to incorporate the two-dimensional heat flow would give more accurate predictions of the actual gradient that could be expected in real casting, not just the trends shown.

Closer investigation of the factors described in sections 7.1.1–7.1.4 would also be important to improve accuracy, looking in detail at how G_L is precisely calculated in the model, including the exact relationship between G_L, the heater temperatures and the liquidus and solidus positions. The introduction of faster algorithms to model the heat flow would also be beneficial.

References:

Alaruri, S., Bianchini, L. and Brewington, A. (1998) Effective spectral emissivity measurements of superalloys and YSZ thermal barrier coating at high temperatures using a 1.6μm single wavelength pyrometer. **Optics and Lasers in Engineering,** 30: 77-91

Bondarenko, Y. A. and Kablov, E. N. (2002). Directional crystallization of high-temperature alloys with elevated temperature gradient. **Metal Science and Heat Treatment,** 44: 288-291

Bradley, D. and Entwistle, A.G. (1961) Determination of the emissivity, for total radiation, of small diameter platinum-10% rhodium wires in the temperature range 600-1450°C. **British Journal of Applied Physics,** 12: 708-711

Brandes, E.A. and Brooke, G.B. (eds.) (1992) **Smithells Metal Reference Book.** 7th ed. Oxford: Butterworths-Heinemann.

Dai, H.J., D'souza, N. and Dong, H.B. (2011) Grain selection in spiral selectors during investment casting of SX Turbine blades: Part 1. experimental investigation. **Metallurgical and Materials Transactions A,**

Deemyad, S. and Silvera, I.F. (2008) Temperature dependence of the emissivity of platinum in the IR. **Review of Scientific Instruments,** 79 (086105): 1-2

Dong, H.B. (2007) Analysis of grain selection during directional solidification of gas turbine blades. **Proceedings of the World Congress on Engineering**, 2

Dong, H.B., Yang, X.L. and Lee, P.D. (2004) Simulation of equiaxed growth ahead of an advancing columnar front in directionally solidified Ni-based superalloys. **Journal of Materials Science,** 39: 7207-7212

D'souza, N., Jennings, P.A., Yang, X.L., Dong, H.B. et al. (2005) Seeding of single-crystal superalloys – role of constitutional undercooling and primary dendrite orientation on stray-grain nucleation and growth. **Metallurgical and Materials Transactions B,** 36B: 657-665

Duan, Q., Luan, Q., Liu, J. and Peng, L. (2010) Microstructure and mechanical properties of directionally solidified high-Nb containing Ti-Al alloys. **Materials and Design,** 31: 3499-3503

Elliot, A.J., and Pollock, T.M., (2007) Thermal analysis of the Bridgman and liquid-metal-cooled directional solidification investment casting processes. **Metallurgical and Materials Transactions A,** 38A: 871-882

Elliot, A.J., Tin, S., King, W.T., Huang, S.C., Gigliotti, M.F.X. and Pollock, T.M. (2004) Directional solidification of large superalloy castings with radiation and liquid-metal cooling: a comparative assessment. **Metallurgical and Materials Transactions A,** 35A: 3221-3231

Elsden, G., (sales@lowdenlimited.co.uk), (4 March 2010) **Re: Graphite Foil F201?.** e-mail to J. MacDonald (jem672@bham.ac.uk) (Personal communication)

Esaka, H., Shinozuka, K., Tamura, M. (2005) Analysis of single crystal casting process taking into account the shape of pigtail. **Materials Science and Engineering A,** (413–414): 151–155

Fu, T.W. and Wilcox, W.R. (1980) Influence of insulation on stability of interface shape and position in the vertical Bridgman-Stockbarger technique. **Journal of Crystal Growth,** 48: 416-424

Gell, M., Duhl, D.N. and Giamei, A.F. (1980) The development of single crystal superalloy turbine blades. **Superalloys:** 205-214

Giulietti, D. and Lucchesi, M. (1981) Emissivity and absorptivity measurements on some high-purity metals at low temperature. **Journal of Physics D: Applied Physics,** 14: 877-881

Green, N.R. (2011) Personal communication, Birmingham University.

Incropera, F.P., DeWitt, D.P., Bergman, T.L. and Lavine, A.S. (2007) **Fundamentals of Heat and Mass Transfer.** 6th ed. Wiley.

Karunaratne, M.S.A., Rae, C.M.F. and Reed, R.C. (2001) On the microstructural instability of an experimental nickel-based single crystal superalloy. **Metallurgical and Materials Transactions A,** 32A: 2409-2421

Kermanpur, A., Mehrara, M., Varahram, N., and Davami, P. (2008) Improvement of grain structure and mechanical properties of a land based gas turbine blade directionally solidified with liquid metal cooling process. **Materials Science and Technology,** 24 (1): 100-106

Kermanpur, A., Varahram, N., Davami, P., and Rappaz, M. (2000) Thermal and grain-structure simulation in a land-based turbine blade directionally solidified with the liquid metal cooling process. **Metallurgical and Materials Transactions B,** 31B: 1293-1304

Konter, M., Kats, E., Hofmann, N. (2000) A novel casting process for single crystal gas turbine components. **Superalloys**: 189-200

Kostanovskii, A.V., Zeodinov, M. G. And Kostanovskaya, M.E. (2005) The determination of thermal conductivity and emissivity of graphite at high temperatures. **High Temperature,** 43 (5): 793-795

Liu, L., Huang, T., Qu, M. et al. (2010) High thermal gradient directional solidification and its application in the processing of nickel-based superalloys, **Journal of Materials Processing Technology**: 159-165

Matsushita, T., Fecht, H.J., Wunderlich, R.K. et al. (2009) Studies of the thermophysical properties of commercial CMSX-4 alloy. **Journal of Chemical Engineering Data,** 54: 2584-2592

Mattie, S., Masclet, P. and Herve, P. (1989) Study of complex refractive indices of gold and copper using emissivity measurements. **Infrared Physics,** 29 (6): 991-994

Orlov, M.R. (2008) Pore formation in single-crystal turbine rotor blades during directional solidification. **Russian Metallurgy (Metally),** 2008 (1):70-75

Pollock, T.M., Murphy, W.H., Goldman, E.H. et al. (1992) Grain defect formation during directional solidification on nickel base single crystals. **Superalloys:** 125-134

Reed, R.C. (2006) **The Superalloys: Fundamentals and Applications.** Cambridge: Cambridge University Press.

Reynolds, P.M. (1961) Spectral emissivity of 99.7% aluminium between 200 and 540°C. **British Journal of Applied Physics,** 12: 111-114

Seo, S.M., Kim, I.S., Lee, J.H. et al. (2009) Grain structure and texture evolutions during single crystal casting of the Ni-base superalloy CMSX-4. **Metallurgy and Materials Int.,** 15 (3): 391-398

Soorya, A. (Jul-Aug 2010) **Numerical Calculation of View Factors in a DS Furnace.** Unpublished, University of Birmingham

Tin, S. and Pollock, T.M. (2003) Stabilisation of thermosolutal convective instabilities in Ni-based single-crystal superalloys: carbide precipitation and rayleigh numbers. **Metallurgical and Materials Transactions A,** 34A: 1953-1967

Toloraiya, V. N., Orekhov, N. G., and Kablov, E.N. (2002) Advanced method for single crystal casting of turbine blades for gas turbine engines and plants. **Metal Science and Heat Treatment,** 44 (7-8): 279-283

Wang, W., Lee, P.D. and McLean, M. (2003) A model of solidification microstructures in nickel-based superalloys: predicting primary dendrite spacing selection. **Acta Materialia,** 51: 2971–2987

Window, B. and Harding, G. (1981) Thermal emissivity of Copper. **Journal of Optical Society of America,** 71 (3): 354-357

Zhang, J. and Lou, L. (2007) Directional solidification assisted by liquid metal cooling. **Journal of Materials Science and Technology,** 23 (3): 289-300